K^+N Elastic Scatterings for Estimation of the In-Medium Quark Condensate with Strange Quarks

Yutaro Iizawa, Daisuke Jido ⓘ*, and Stephan Hübsch

Department of Physics, Tokyo Institute of Technology, Meguro, Tokyo 152-8551, Japan
*E-mail: jido@phys.titech.ac.jp

....
We revisit the low-energy K^+N elastic scatterings in the context of the in-medium quark condensate with strange quarks. The chiral ward identity connects the in-medium quark condensate to the soft limit value of the pseudoscalar correlation function evaluated in nuclear matter. The in-medium correlation function of the pseudoscalar fields with strangeness describes in-medium kaon propagation and is obtained by kaon–nucleon scattering amplitudes in the low-density approximation. We construct the kaon–nucleon scattering amplitudes in chiral perturbation theory up to the next-to-leading order and add some terms of the next-to-next-to-leading order with the strange quark mass to improve expansion of the strange quark sector. We also consider the effect of a possible broad resonance state around $P_{lab} = 600\,\text{MeV}/c$ for $I = 0$ reported in the previous study. The low-energy constants are determined by existing K^+N scattering data. We obtain good reproduction of the K^+p scattering amplitude by chiral perturbation theory, while the description of the KN amplitude with $I = 0$ is not so satisfactory due to the lack of low-energy data. Performing analytic continuation of the scattering amplitudes obtained by chiral perturbation theory to the soft limit, we estimate the in-medium strange quark condensate.
....
Subject Index   B60, D32, D33

1. Introduction

Chiral symmetry is one of the symmetries of quantum chromodynamics (QCD) of the fundamental theory for strong interactions and is broken dynamically at low energies as a phase transition phenomenon. In the vacuum phase transition, the quark condensate $\langle \bar{q}q \rangle$ is one of the order parameters for the symmetry breaking. In the case of the exact chiral symmetry, the value of the quark condensate is zero when chiral symmetry is manifest, and after the symmetry breaking it becomes finite. This is called the dynamical breaking of chiral symmetry (DBχS). In extreme environments, e.g. high temperature and/or high density, the broken chiral symmetry is expected to be fully restored.

In order to confirm how DBχS takes place phenomenologically, we investigate the partial restoration of the chiral symmetry in nuclear matter. There the magnitude of the quark condensate is expected to decrease as chiral symmetry is restored in nuclear matter. Since the quark condensate is not directly observable, it is necessary to obtain the information on the quark condensate through the experimental values of hadrons in nuclei, such as hadron–nucleus scatterings and bound states of hadrons in nuclei. Of particular interest is the in-medium property of the Nambu–Goldstone boson (NG boson) such as the pion. The NG bosons appear to be associated with DBχS. Hence the properties of the NG bosons should be sensitive to the nature of DBχS. The partial restoration of DBχS has been studied especially for pions in the nucleus,

which extracts the in-medium quark condensate $\langle \bar{u}u + \bar{d}d \rangle$ for two flavors. From the observations of deeply bound pionic atoms [1] and the low-energy pion–nucleus elastic scatterings [2], the isovector scattering length of the π–nucleus system b_1^* was extracted. Comparing b_1^* and that in the πN system b_1 based on theoretical considerations [3,4], it is suggested that chiral symmetry is restored about 30% at normal nuclear density. Theoretically, the restoration of chiral symmetry in nuclear matter was predicted by a model-independent low-density theorem [5,6]. In this relation, the sign of the experimental $\sigma_{\pi N}$ term or the theoretical c_1 parameter of chiral perturbation theory determines whether the magnitude of the quark condensate increases or decreases in nuclear matter. Since the $\sigma_{\pi N}$ term extracted from the experimental data of low-energy πN scatterings [7–12] is found to have a positive sign, the quark condensate should decrease in nuclear matter. Similar results are obtained by in-medium chiral perturbation theory [13–15], which is developed by Refs. [16,17].

From the systematic point of view, we study the quark condensate with strange components in nuclear matter in this paper. As with $\langle \bar{u}u + \bar{d}d \rangle$, a theoretical calculation for the low-density relation of $\langle \bar{u}u + \bar{s}s \rangle$ is performed based on the correlation function approach developed in Refs. [4,14]. There the in-medium quark condensate $\langle \bar{u}u + \bar{s}s \rangle$ is written in terms of the kaon–nucleon scattering amplitude at the soft limit in the linear density approximation. We use chiral perturbation theory to extrapolate the scattering amplitude to the soft limit. The low-energy constants (LECs) in the amplitude are determined from experimental data as well as the $\sigma_{\pi N}$ term. The current approach is a complementary method to the evaluation of the quark condensate by using the Feynman–Hellmann theorem where the quark condensate is obtained by taking the derivative of the nucleon energy density with respect to the quark mass [13,16–18].

We make good use of the $K^+ N$ scattering in order to determine the LECs. For determining the LECs, $K^+ N$ scatterings are preferable over $K^- N$ scatterings since in the $\bar{K} N$ system the $\Lambda(1405)$ resonance appears below the threshold with a narrow decay width, while such a resonance does not exist in the $K^+ N$ system. The $K^+ N$ scattering at low energy has been studied for a long time [19–23]. Recently, Ref. [24] carried out the construction of the $K^+ N$ scattering amplitude using chiral perturbation theory up to the next-to-leading order, in which some terms were missing. Reference [25] constructed the $K^+ N$ scattering amplitude using the chiral unitary approach and discussed the presence of a broad resonance state with $I = 0, S = +1$ around $P_{\text{lab}} = 600 \, \text{MeV}/c$. For the purpose of determining the LECs, the $K^+ N$ scatterings need to be described by chiral perturbation theory. In our calculation, we construct $K^+ N$ scattering amplitudes using the chiral perturbation theory up to the next-to-leading order and some terms from the next-to-next order, which includes the strange quark mass [26], and determine the LECs using scattering data. With the determined LECs we estimate the low-density behavior of the quark condensate with strange quarks in nuclear matter.

The structure of this paper is as follows. In Section 2, we derive a relation to the in-medium quark condensate with strange quarks and the KN scattering amplitude based on the correlation function approach [4,14,15] and the low-density theorem [5,6]. In Section 3, we construct the $K^+ N$ scattering amplitudes using chiral perturbation theory. In Section 4, we determine the LECs so as to reproduce the existing $K^+ N$ scattering data. Using the determined LECs, we discuss the behavior of the in-medium quark condensate with strange quarks. The quark condensates in hyperon matter and SU(3) flavor symmetric baryonic matter are also discussed.

Moreover, we evaluate the wave function renormalization of the in-medium kaon. In Section 5, we summarize the results of this paper.

2. In-medium quark condensate with strange quarks

As mentioned in the introduction, the purpose of this paper is to estimate the extended quark condensate to flavor SU(3). In this section, we describe the quark condensate in the nuclear medium based on the correlation function approach developed in Refs. [4,14,15] and the low-density theorem [5,6]. In this paper, we assume isospin symmetric nuclear matter.

2.1. *Correlation function approach*

Following Refs. [4,14,15], we calculate the divergence of the time-ordered product of the axial-vector current A_μ and the pseudoscalar field P given as

$$\partial^\mu \mathbf{T}\left[A_\mu^\dagger(x)P(0)\right] = \mathbf{T}\left[\partial^\mu A_\mu^\dagger(x)P(0)\right] + \delta(x_0)\left[A_0^\dagger(x), P(0)\right] \tag{1}$$

where the axial-vector current $A_\mu(x)$ and the pseudoscalar field $P(x)$ are defined in terms of the up and strange quark fields as

$$A_\mu(x) = \frac{1}{\sqrt{2}}\bar{s}(x)\gamma_\mu\gamma_5 u(x), \tag{2}$$

$$P(x) = \sqrt{2}i\bar{s}(x)\gamma_5 u(x), \tag{3}$$

respectively. The axial-vector current is one of the Noether currents associated with the SU(3) chiral transformation and the pseusodcalar field appears in the partially conserved axial current (PCAC) relation

$$\partial^\mu A_\mu(x) = \frac{m + m_s}{2}P(x), \tag{4}$$

with explicit chiral symmetry breaking by the quark masses. Here m and m_s are the current quark masses of the light and strange quarks, respectively, with the isospin symmetry $m = m_u = m_d$. The pseudoscalar field is transformed under the axial transformation generated by $Q_5 \equiv \int d^3x A_0^\dagger(x)$ as

$$[Q_5, P(x)] = -iS(x), \tag{5}$$

where the scalar field S is given by

$$S(x) = \bar{u}(x)u(x) + \bar{s}(x)s(x). \tag{6}$$

Evaluating Eq. (1) for the ground state of nuclear matter $|\Omega\rangle$ and introducing the in-medium correlation functions

$$\Pi_{5\mu}(x; \rho) = \left\langle \mathbf{T}A_\mu^\dagger(x)P(0)\right\rangle^* \equiv \langle\Omega|\mathbf{T}A_\mu^\dagger(x)P(0)|\Omega\rangle, \tag{7}$$

$$\Pi(x; \rho) = \left\langle \mathbf{T}P^\dagger(x)P(0)\right\rangle^* \equiv \langle\Omega|\mathbf{T}P^\dagger(x)P(0)|\Omega\rangle, \tag{8}$$

we obtain in the momentum space

$$-iq^\mu \Pi_{5\mu}(q) = \frac{m + m_s}{2}\Pi^{ab}(q) + \int d^3x e^{-i\boldsymbol{q}\cdot\boldsymbol{x}}\left\langle\Omega\left|\left[A_0^\dagger(x), P(0)\right]\right|\Omega\right\rangle. \tag{9}$$

When we take the soft limit $q^\mu \to 0$ for Eq. (9), the left-hand side vanishes since we do not have any zero modes off the chiral limit and the second term of the right-hand side yields the scalar field S by using Eq. (6). Finally, we have the in-medium condensate

$$\langle\bar{u}u + \bar{s}s\rangle^* \equiv \langle\Omega|\bar{u}u + \bar{s}s|\Omega\rangle = -i\frac{m + m_s}{2}\Pi(q = 0; \rho) \tag{10}$$

and the in-vacuum condensate

$$\langle \bar{u}u + \bar{s}s \rangle_0 \equiv \langle 0|\bar{u}u + \bar{s}s|0 \rangle = -i\frac{m + m_s}{2}\Pi(q = 0; \rho = 0). \tag{11}$$

2.2. *Low-density theorem*

In the low-density theorem [5,6], we can expand the in-medium matrix element of an operator $\mathcal{O}$ as

$$\langle \Omega|\mathcal{O}|\Omega \rangle = \langle 0|\mathcal{O}|0 \rangle + \rho\langle N|\mathcal{O}|N \rangle + O(\rho^{n>1}). \tag{12}$$

Applying this theorem to $\Pi(x; \rho)$, we obtain

$$\Pi(x; \rho) = \langle 0|P^\dagger(x)P(0)|0 \rangle + \rho\langle N|P^\dagger(x)P(0)|N \rangle + O(\rho^{n>1}). \tag{13}$$

The matrix element $\langle N|P^\dagger(x)P(0)|N \rangle$ is written by the isospin-averaged kaon–nucleon scattering amplitude $T_{KN}(q)$ using the reduction formula [27] as

$$\text{F.T.}\langle N|P^\dagger(x)P(0)|N \rangle = \frac{i}{q^2 - M_K^2}\frac{G_K^2}{q^2 - M_K^2}\left(-\frac{T_{KN}(q)}{2M_N}\right) \tag{14}$$

where G_K is the in-vacuum coupling defined as $\langle 0|P|K^+ \rangle \equiv G_K$. Finally, with Eqs. (10), (11), (13), and (14), the quark condensate with strange components is given in terms of the isospin-averaged kaon–nucleon scattering amplitude T_{KN} in the soft limit as

$$\frac{\langle \bar{u}u + \bar{s}s \rangle^*}{\langle \bar{u}u + \bar{s}s \rangle_0} = \left(1 + \frac{\rho}{M_K^2}\frac{T_{KN}(q = 0)}{2M_N}\right). \tag{15}$$

Here, in order to evaluate the condensate, it is necessary to take the soft limit for T_{KN}. For this purpose, T_{KN} is constructed using chiral perturbation theory in the next section.

3. Formulation for *KN* amplitudes

3.1. *The chiral Lagrangian*

In order to estimate the in-medium quark condensate with strange quarks, $\langle \bar{u}u + \bar{s}s \rangle^*$, based on Eq. (15), we construct the kaon–nucleon scattering amplitude T_{KN} using chiral perturbation theory. Chiral perturbation theory provides an analytic form of the scattering amplitude as a function of the energy and momentum. This is favorable for the analytic continuation of the scattering amplitude to the soft limit. The soft limit $q_\mu = 0$ is not on the mass shell. Thus, the extrapolation to the soft limit has to be performed without taking the on-shell condition. We determine the low-energy constants from the observed data of the K^+N scattering.

The leading order of the SU(3) meson–baryon chiral Lagrangian reads

$$\mathcal{L}_{MB}^{(1)} = \text{Tr}\left\{\bar{B}(i\slashed{D} - M_0)B)\right\} - \frac{D}{2}\text{Tr}\left\{\bar{B}\gamma^\mu\gamma^5\{u_\mu, B\}\right\} - \frac{F}{2}\text{Tr}\left\{\bar{B}\gamma^\mu\gamma^5[u_\mu, B]\right\}, \tag{16}$$

where M_0 is the baryon mass at the chiral limit, D and F are low-energy constants to be determined by experiments, and the baryon and meson fields, B and Φ, are written in the SU(3) matrix form as

$$\Phi = \begin{pmatrix} \frac{\pi^0}{\sqrt{2}} + \frac{\eta}{\sqrt{6}} & \pi^+ & K^+ \\ \pi^- & -\frac{\pi^0}{\sqrt{2}} + \frac{\eta}{\sqrt{6}} & K^0 \\ K^- & \bar{K}^0 & -\frac{2}{\sqrt{6}}\eta \end{pmatrix}, \tag{17}$$

$$B = \begin{pmatrix} \frac{\Sigma^0}{\sqrt{2}} + \frac{\Lambda}{\sqrt{6}} & \Sigma^+ & p \\ \Sigma^- & -\frac{\Sigma^0}{\sqrt{2}} + \frac{\Lambda}{\sqrt{6}} & n \\ \Xi^- & \Xi^0 & -\frac{2}{\sqrt{6}}\Lambda \end{pmatrix}. \tag{18}$$

Here we use the Coleman–Callan–Wess–Zumino (CCWZ) parametrization of the chiral field U as

$$U = \exp(i\sqrt{2}\Phi/f) \tag{19}$$

where f is a normalization of the meson field Φ and corresponds to the meson decay constant at tree level. The covariant derivative for the baryon field is introduced as

$$D_\mu B = \partial_\mu B + [\Gamma_\mu, B] \tag{20}$$

with the mesonic vector current given as

$$\Gamma_\mu = \frac{1}{2}(\xi^\dagger \partial_\mu \xi + \xi \partial_\mu \xi^\dagger)$$

where $\xi^2 = U$. The mesonic axial-vector current is introduced as

$$u_\mu = i(\xi^\dagger \partial_\mu \xi - \xi \partial_\mu \xi^\dagger). \tag{21}$$

The next-to-leading order (NLO) of the chiral Lagrangian is given by

$$\mathcal{L}_{MB}^{(2)} = b_D \text{Tr}\left\{\bar{B}\{\chi_+, B\}\right\} + b_F \text{Tr}\left\{\bar{B}[\chi_+, B]\right\} + b_0 \text{Tr}\left\{\bar{B}B\right\} \text{Tr}\{\chi_+\} + d_1 \text{Tr}\left(\bar{B}\{u_\mu, [u^\mu, B]\}\right)$$

$$+ d_2 \text{Tr}\left(\bar{B}[u_\mu, [u^\mu, B]]\right) + d_3 \text{Tr}\left(\bar{B}u_\mu\right)\text{Tr}(u^\mu B) + d_4 \text{Tr}\left(\bar{B}B\right)\text{Tr}(u^\mu u_\mu)$$

$$- \frac{g_1}{8M_N^2}\text{Tr}\left(\bar{B}\{u_\mu, [u_\nu, \{D^\mu, D^\nu\}B]\}\right) - \frac{g_2}{8M_N^2}\text{Tr}\left(\bar{B}[u_\mu, [u_\nu, \{D^\mu, D^\nu\}B]]\right)$$

$$- \frac{g_3}{8M_N^2}\text{Tr}(\bar{B}u_\mu)\text{Tr}(u_\nu, \{D^\mu, D^\nu\}B) - \frac{g_4}{8M_N^2}\text{Tr}(\bar{B}\{D^\mu, D^\nu\}B)\text{Tr}(u_\mu u_\nu)$$

$$- \frac{h_1}{4}\text{Tr}\left(\bar{B}[\gamma^\mu, \gamma^\nu]Bu_\mu u_\nu\right) - \frac{h_2}{4}\text{Tr}\left(\bar{B}[\gamma^\mu, \gamma^\nu]u_\mu[u_\nu, B]\right)$$

$$- \frac{h_3}{4}\text{Tr}\left(\bar{B}[\gamma^\mu, \gamma^\nu]u_\mu\{u_\nu, B\}\right) - \frac{h_4}{4}\text{Tr}(\bar{B}[\gamma^\mu, \gamma^\nu]u_\mu)\text{Tr}(u_\nu B) + \text{h.c.} \tag{22}$$

where b_i, d_i, g_i, and h_i are the LECs of NLO. The terms that include b_i and d_i appear in the typical flavor SU(3) chiral Lagrangian such as in Refs. [24,28], while the terms that include g_i and h_i are introduced as the extension of the flavor SU(2) chiral Lagrangian and used in Ref. [25]. This Lagrangian is consistent with the most general form of the next-to-leading order shown in Refs. [29,30].

The scalar ($s = s^a \lambda^a$, $a = 0, 1, 2\ldots8$) and pseudoscalar ($p = p^a \lambda^a$, $a = 0, 1, 2\ldots8$) sources are contained in $\chi_\pm$ as

$$\chi_\pm = \xi \chi^\dagger \xi \pm \xi^\dagger \chi \xi^\dagger \tag{23}$$

through χ defined as

$$\chi = 2B_0(s + ip), \tag{24}$$

where B_0 is a low-energy constant. The current quark masses are introduced through the external scalar field by setting

$$s = \text{diag}(m, m, m_s), \tag{25}$$

with the isospin-averaged quark mass m and the strange quark mass m_s. The low-energy constant B_0 is fixed with the current quark masses by the kaon mass with the relation $M_K^2 = B_0(m + m_s)$ in this work.

In order to improve extrapolation in the strange quark sector, we introduce some terms of the next-to-next-to-leading order (NNLO) of the chiral Lagrangian [29], which contain the strange

quark mass m_s in χ_- as

$$\mathcal{L}_{MB}^{(3)} = v_D \operatorname{Tr}\left(\bar{B}\{\chi_-, \gamma_5 B\}\right) + v_F \operatorname{Tr}\left(\bar{B}[\chi_-, \gamma_5 B]\right)$$

$$+ w_1 \operatorname{Tr}\left(\bar{B}\gamma_\mu B[\chi_-, u^\mu]\right) + w_2 \operatorname{Tr}\left(\bar{B}[\chi_-, u^\mu]\gamma_\mu B\right)$$

$$+ w_3 \left[\operatorname{Tr}\left(\bar{B}u^\mu\right)\operatorname{Tr}\left(\chi_-\gamma_\mu B\right) - \operatorname{Tr}\left(\bar{B}\chi_-\right)\operatorname{Tr}\left(u^\mu\gamma_\mu B\right)\right] \tag{26}$$

where v_i and w_i are the LECs. There are other NNLO terms containing derivatives instead of the quark masses. As discussed in Ref. [26], mathematically the expansions in terms of the quark mass and the NG meson momentum are independent, although physically they are correlated through the Gell-Mann–Oakes–Renner relation. Here we would take the quark mass expansion more seriously.

3.2. Scattering amplitude

To determine the LECs from the experimental data, we are allowed to take the on-shell condition on the external particles. In such a case, the T-matrix for kaon and nucleon scattering is generally written as

$$T_{KN}(s, t) = \bar{u}(\boldsymbol{p}_4, s_4)\left[A(s, t) + \frac{1}{2}(\not{p}_1 + \not{p}_3)B(s, t)\right]u(\boldsymbol{p}_2, s_2), \tag{27}$$

where p_1 and p_2 denote the initial K^+ and nucleon momenta, respectively, while p_3 and p_4 stand for the final kaon and nucleon momenta, $u(\boldsymbol{p}, s)$ is a Dirac spinor with 3-momentum $\boldsymbol{p}$ and spin s, which is normalized by $\bar{u}(\boldsymbol{p}, s)u(\boldsymbol{p}, s') = 2M_N\delta_{ss'}$ with nucleon mass M_N, and $A(s, t)$ and $B(s, t)$ are two Lorentz-invariant functions of the two independent Mandelstam variables $s = (p_1 + p_2)^2$ and $t = (p_1 - p_3)^2$.

The $K^+ N$ scattering amplitudes in the particle basis $T_{K^+ p \to K^+ p}$, $T_{K^+ n \to K^+ n}$, and $T_{K^+ n \to K^0 p}$ are constructed by those in the isospin basis T^I $(I = 0, 1)$ as

$$T_{K^+ p \to K^+ p} = T^{I=1}, \tag{28}$$

$$T_{K^+ n \to K^+ n} = \frac{1}{2}\left(T^{I=1} + T^{I=0}\right), \tag{29}$$

$$T_{K^+ n \to K^0 p} = \frac{1}{2}\left(T^{I=1} - T^{I=0}\right). \tag{30}$$

Let us take the center-of-mass (c.m.) frame for partial wave decomposition. There we write the T-matrix in terms of non-spin-flip amplitude f and spin-flip amplitude g as

$$T(s, t) = \chi^\dagger(\lambda_4)\left[f(W, \theta) - i(\boldsymbol{\sigma} \cdot \hat{\boldsymbol{n}})g(W, \theta)\right]\chi(\lambda_2) \tag{31}$$

where W and θ are the total energy of the system and the scattering angle between $\boldsymbol{p}_1$ and $\boldsymbol{p}_3$ in the center-of-mass (c.m.) frame, respectively, $\hat{\boldsymbol{n}}$ is the normal vector of the scattering plane defined by

$$\hat{\boldsymbol{n}} = \frac{\boldsymbol{p}_3 \times \boldsymbol{p}_1}{|\boldsymbol{p}_3 \times \boldsymbol{p}_1|}, \tag{32}$$

and $\chi(\lambda)$ is the Pauli spinor of a nucleon with helicity λ.

From Eqs. (27) and (31), we obtain the relation of the Lorentz-invariant amplitudes A, B and the c.m. amplitudes f, g as

$$f(W, \theta) = (E_N + M_N)(A + \omega_K B) + k^2 B + \frac{(E_N + M_N + \omega_K)B - A}{E_N + M_N}k^2 \cos\theta, \tag{33}$$

$$g(W, \theta) = -\frac{(E_N + M_N + \omega_K)B - A}{E_N + M_N} k^2 \sin \theta, \tag{34}$$

where E_N, ω_K, and k stand for the nucleon energy, kaon energy, and kaon momentum in the center-of-mass frame, respectively. The amplitudes f and g are decomposed into partial waves with the Legendre polynomial $P_\ell(x)$ as

$$f(W, \theta) = \sum_{\ell=0}^{\infty} f_\ell(W) P_\ell(\cos \theta), \tag{35}$$

$$g(W, \theta) = \sum_{\ell=0}^{\infty} g_\ell(W) \sin \theta \frac{dP_\ell(\cos \theta)}{d \cos \theta}. \tag{36}$$

We introduce the amplitude of the total angular momentum $j = \ell \pm \frac{1}{2}$, $T_{\ell \pm}$ as

$$f_\ell(W) = (\ell + 1)T_{\ell+}(W) + \ell T_{\ell-}(W), \tag{37}$$

$$g_\ell(W) = T_{\ell+}(W) - T_{\ell-}(W), \tag{38}$$

or equivalently

$$T_{\ell+}(W) = \frac{1}{2\ell + 1}(f_\ell(W) + \ell g_\ell(W)), \tag{39}$$

$$T_{\ell-}(W) = \frac{1}{2\ell + 1}(f_\ell(W) - (\ell + 1)g_\ell(W)). \tag{40}$$

By taking the average of the initial nucleon spins and the summation of the final nucleon spins, the differential cross section in the center-of-mass frame is calculated as

$$\frac{d\sigma}{d\Omega} = \frac{1}{64\pi^2 s} \left(|f(W, \theta)|^2 + |g(W, \theta)|^2 \right). \tag{41}$$

By integrating the differential cross section with respect to the solid angle Ω, we obtain the total cross section as

$$\sigma = \frac{1}{32\pi s} \int d \cos \theta \left(|f(W, \theta)|^2 + |g(W, \theta)|^2 \right). \tag{42}$$

3.3. K^+N scattering amplitude in chiral perturbation theory

In this section, we construct the tree-level amplitude of the K^+N elastic scattering using the chiral perturbation theory. Here we consider the following four terms:

$$T^{KN} = T_{\mathrm{WT}} + T_{\mathrm{Born}} + T_{\mathrm{NLO}} + T_{\mathrm{NNLO}}. \tag{43}$$

The leading-order contribution contains the amplitudes of the contact Weinberg–Tomozawa interaction T_{WT} and the u-channel Born terms of the hyperons T_{Born} with the KYN Yukawa interactions given in Eq. (16). The loop diagrams contribute from the next-to-next-to-leading order (NNLO).

The invariant amplitudes for the Weinberg–Tomozawa diagram in the isospin basis are calculated from the leading-order Lagrangian (16) as

$$T_{\mathrm{WT}}^{I=0} = 0, \tag{44a}$$

$$T_{\mathrm{WT}}^{I=1} = \frac{1}{2F_K^2} \bar{u}(\boldsymbol{p}_4, s_4)(\not{p}_1 + \not{p}_3)u(\boldsymbol{p}_2, s_2), \tag{44b}$$

and their corresponding invariant amplitudes read

$$A_{\mathrm{WT}}^{I=0} = B_{\mathrm{WT}}^{I=0} = A_{\mathrm{WT}}^{I=1} = 0, \tag{45a}$$

$$B_{\mathrm{WT}}^{I=1} = \frac{1}{F_K^2}, \tag{45b}$$

with the kaon decay constant F_K. The invariant amplitudes for the u-channel Born terms in the isospin basis are evaluated as

$$T_{\mathrm{Born}}^{I=0} = -\frac{3}{4}\frac{(D-F)^2}{F_K^2}\bar{u}(\boldsymbol{p}_4, s_4)\slashed{p}_1\gamma_5\frac{M_\Sigma + (\slashed{p}_2 - \slashed{p}_3)}{M_\Sigma^2 - (p_2 - p_3)^2 - i\epsilon}\slashed{p}_3\gamma_5 u(\boldsymbol{p}_2, s_2)$$

$$+ \frac{1}{12}\frac{(3F+D)^2}{F_K^2}\bar{u}(\boldsymbol{p}_4, s_4)\slashed{p}_1\gamma_5\frac{M_\Lambda + (\slashed{p}_2 - \slashed{p}_3)}{M_\Lambda^2 - (p_2 - p_3)^2 - i\epsilon}\slashed{p}_3\gamma_5 u(\boldsymbol{p}_2, s_2), \tag{46a}$$

$$T_{\mathrm{Born}}^{I=1} = -\frac{1}{4}\frac{(D-F)^2}{F_K^2}\bar{u}(\boldsymbol{p}_4, s_4)\slashed{p}_1\gamma_5\frac{M_\Sigma + (\slashed{p}_2 - \slashed{p}_3)}{M_\Sigma^2 - (p_2 - p_3)^2 - i\epsilon}\slashed{p}_3\gamma_5 u(\boldsymbol{p}_2, s_2)$$

$$- \frac{1}{12}\frac{(3F+D)^2}{F_K^2}\bar{u}(\boldsymbol{p}_4, s_4)\slashed{p}_1\gamma_5\frac{M_\Lambda + (\slashed{p}_2 - \slashed{p}_3)}{M_\Lambda^2 - (p_2 - p_3)^2 - i\epsilon}\slashed{p}_3\gamma_5 u(\boldsymbol{p}_2, s_2) \tag{46b}$$

with the Σ baryon mass M_Σ and the Λ baryon mass M_Λ. The corresponding invariant amplitudes read

$$A_{\mathrm{Born}}^{I=0} = \frac{3}{4}\frac{(D-F)^2}{F_K^2}\frac{(M_N+M_\Sigma)\left(M_N^2 - u\right)}{u - M_\Sigma^2} - \frac{1}{12}\frac{(3F+D)^2}{F_K^2}\frac{(M_N+M_\Lambda)\left(M_N^2 - u\right)}{u - M_\Lambda^2}, \tag{47a}$$

$$B_{\mathrm{Born}}^{I=0} = -\frac{3}{4}\frac{(D-F)^2}{F_K^2}\frac{u + M_N^2 + 2M_\Sigma M_N}{u - M_\Sigma^2} + \frac{1}{12}\frac{(3F+D)^2}{F_K^2}\frac{u + M_N^2 + 2M_\Lambda M_N}{u - M_\Lambda^2}, \tag{47b}$$

$$A_{\mathrm{Born}}^{I=1} = \frac{1}{4}\frac{(D-F)^2}{F_K^2}\frac{(M_N+M_\Sigma)\left(M_N^2 - u\right)}{u - M_\Sigma^2} + \frac{1}{12}\frac{(3F+D)^2}{F_K^2}\frac{(M_N+M_\Lambda)\left(M_N^2 - u\right)}{u - M_\Lambda^2}, \tag{47c}$$

$$B_{\mathrm{Born}}^{I=1} = -\frac{1}{4}\frac{(D-F)^2}{F_K^2}\frac{u + M_N^2 + 2M_\Sigma M_N}{u - M_\Sigma^2} - \frac{1}{12}\frac{(3F+D)^2}{F_K^2}\frac{u + M_N^2 + 2M_\Lambda M_N}{u - M_\Lambda^2}, \tag{47d}$$

with the Mandelstam variable $u = (p_2 - p_3)^2$. We will use the isospin-averaged physical baryon masses for the calculation.

The next-to-leading order of the K^+N scattering amplitudes for $I = 0, 1$ is calculated from Lagrangian (22) as

$$T_{\mathrm{NLO}}^I = \left[\frac{4B_0}{F_K^2}(\hat{m} + m_s)b^I + \frac{2}{F_K^2}(p_1 \cdot p_3)d^I + \frac{(p_2 \cdot p_1)(p_2 \cdot p_3) + (p_4 \cdot p_1)(p_4 \cdot p_3)}{2M_N^2 F_K^2}g^I\right]$$

$$\times \bar{u}(\boldsymbol{p}_4, s_4)u(\boldsymbol{p}_2, s_2) - \frac{h^I}{2F_K^2}p_1^\mu p_3^\nu \bar{u}(\boldsymbol{p}_4, s_4)[\gamma_\mu, \gamma_\nu]u(\boldsymbol{p}_2, s_2), \tag{48}$$

where we have introduced the LECs for the NLO in the isospin basis, b^I, d^I, g^I, and h^I, which are written in terms of the LECs b_i, d_i, g_i, and h_i appearing in Eq. (22) as

$$b^{I=0} = b_0 - b_F, \quad b^{I=1} = b_0 + b_D, \tag{49a}$$

$$d^{I=0} = 2d_1 + d_3 - 2d_4, \quad d^{I=1} = -2d_2 - d_3 - 2d_4, \tag{49b}$$

$$g^{I=0} = 2g_1 + g_3 - 2g_4, \quad g^{I=1} = -2g_2 - g_3 - 2g_4, \tag{49c}$$

$$h^{I=0} = h_1 + h_2 + h_3 + h_4, \quad h^{I=1} = h_1 - h_2 - h_3 - h_4. \tag{49d}$$

The corresponding invariant amplitudes to Eq. (48) read

$$A_{\mathrm{NLO}}^I = \frac{4B_0}{F_K^2}(m + m_s)b^I + \frac{2}{F_K^2}(p_1 \cdot p_3)d^I$$

$$+ \frac{(p_2 \cdot p_1)(p_2 \cdot p_3) + (p_4 \cdot p_1)(p_4 \cdot p_3)}{2M_N^2 F_K^2}g^I + \frac{p_1 \cdot (p_2 + p_4)}{F_K^2}h^I \tag{50a}$$

$$B_{\mathrm{NLO}}^I = -\frac{2M_N}{F_K^2}h^I. \tag{50b}$$

The K^+N scattering amplitudes obtained by using the NNLO chiral Lagrangian (26) for $I = 0, 1$ are given by

$$T_{\mathrm{NNLO}}^{I=0} = \frac{3(D-F)(v_D - v_F)M_K^2}{F_K^2}$$

$$\times \bar{u}(\boldsymbol{p}_4, s_4) \left(\gamma_5 \frac{M_\Sigma + \not{p}_2 - \not{p}_3}{M_\Sigma^2 - (p_2 - p_3)^2} \not{p}_3 \gamma_5 - \not{p}_1 \gamma_5 \frac{M_\Sigma + \not{p}_2 - \not{p}_3}{M_\Sigma^2 - (p_2 - p_3)^2} \gamma_5 \right) u(\boldsymbol{p}_2, s_2)$$

$$- \frac{(D+3F)(v_D + 3v_F)M_K^2}{3F_K^2}$$

$$\times \bar{u}(\boldsymbol{p}_4, s_4) \left(\gamma_5 \frac{M_\Lambda + \not{p}_2 - \not{p}_3}{M_\Lambda^2 - (p_2 - p_3)^2} \not{p}_3 \gamma_5 - \not{p}_1 \gamma_5 \frac{M_\Lambda + \not{p}_2 - \not{p}_3}{M_\Lambda^2 - (p_2 - p_3)^2} \gamma_5 \right) u(\boldsymbol{p}_2, s_2)$$

$$- \frac{4(w_1 + w_2 - w_3)M_K^2}{F_K^2} \bar{u}(\boldsymbol{p}_4, s_4)(\not{p}_1 + \not{p}_3)u(\boldsymbol{p}_2, s_2), \tag{51a}$$

$$T_{\mathrm{NNLO}}^{I=1} = \frac{(D-F)(v_D - v_F)M_K^2}{F_K^2}$$

$$\times \bar{u}(\boldsymbol{p}_4, s_4) \left(\gamma_5 \frac{M_\Sigma + \not{p}_2 - \not{p}_3}{M_\Sigma^2 - (p_2 - p_3)^2} \not{p}_3 \gamma_5 - \not{p}_1 \gamma_5 \frac{M_\Sigma + \not{p}_2 - \not{p}_3}{M_\Sigma^2 - (p_2 - p_3)^2} \gamma_5 \right) u(\boldsymbol{p}_2, s_2)$$

$$+ \frac{(D+3F)(v_D + 3v_F)M_K^2}{3F_K^2}$$

$$\times \bar{u}(\boldsymbol{p}_4, s_4) \left(\gamma_5 \frac{M_\Lambda + \not{p}_2 - \not{p}_3}{M_\Lambda^2 - (p_2 - p_3)^2} \not{p}_3 \gamma_5 - \not{p}_1 \gamma_5 \frac{M_\Lambda + \not{p}_2 - \not{p}_3}{M_\Lambda^2 - (p_2 - p_3)^2} \gamma_5 \right) u(\boldsymbol{p}_2, s_2)$$

$$- \frac{4(w_1 - w_2 + w_3)M_K^2}{F_K^2} \bar{u}(\boldsymbol{p}_4, s_4)(\not{p}_1 + \not{p}_3)u(\boldsymbol{p}_2, s_2). \tag{51b}$$

These amplitudes are quark mass corrections of the Weinberg–Tomozawa interaction and u-channel Born terms. The corresponding invariant amplitudes to Eq. (51) read

$$A_{\mathrm{NNLO}}^{I=0} = \frac{6(D-F)v_- M_K^2}{F_K^2} \frac{(p_1 \cdot p_4) + (p_2 \cdot p_3) - M_K^2}{u - M_\Sigma^2}$$

$$- \frac{2(D+3F)v_+ M_K^2}{3F_K^2} \frac{(p_1 \cdot p_4) + (p_2 \cdot p_3) - M_K^2}{u - M_\Lambda^2} \tag{52a}$$

$$B_{\mathrm{NNLO}}^{I=0} = -\frac{6(D-F)v_- M_K^2}{F_K^2} \frac{M_N + M_\Sigma}{u - M_\Sigma^2}$$

$$+ \frac{2(D+3F)v_+ M_K^2}{3F_K^2} \frac{M_N + M_\Lambda}{u - M_\Lambda^2} - \frac{8 M_K^2 w^{I=0}}{F_K^2} \tag{52b}$$

$$A_{\mathrm{NNLO}}^{I=1} = \frac{2(D-F)v_- M_K^2}{F_K^2} \frac{(p_1 \cdot p_4) + (p_2 \cdot p_3) - M_K^2}{u - M_\Sigma^2}$$

$$+ \frac{2(D+3F)v_+ M_K^2}{3F_K^2} \frac{(p_1 \cdot p_4) + (p_2 \cdot p_3) - M_K^2}{u - M_\Lambda^2} \tag{52c}$$

$$B_{\mathrm{NNLO}}^{I=1} = -\frac{2(D-F)v_- M_K^2}{F_K^2} \frac{M_N + M_\Sigma}{u - M_\Sigma^2}$$

$$- \frac{2(D+3F)v_+ M_K^2}{3F_K^2} \frac{M_N + M_\Lambda}{u - M_\Lambda^2} - \frac{8 M_K^2 w^{I=1}}{F_K^2}, \tag{52d}$$

where we have introduced the LECs for the NNLO as

$$v_- = v_D - v_F, \quad v_+ = v_D + 3v_F, \tag{53a}$$

$$w^{I=0} = w_1 - w_2 + w_3, \quad w^{I=1} = w_1 + w_2 - w_3. \tag{53b}$$

The low-energy constants $v_\pm$ in the next-to-next-to-leading order of the Lagrangian are included in both isospin channels.

Applying the isospin-averaged kaon–nucleon amplitude to Eq. (15), we obtain the quark condensate in terms of the LECs defined in chiral perturbation theory as

$$\frac{\langle \bar{u}u + \bar{s}s \rangle^*}{\langle \bar{u}u + \bar{s}s \rangle_0} = \left(1 + \frac{\rho}{2M_N M_K^2} \frac{3T^{I=1}(q=0) + T^{I=0}(q=0)}{4} \right)$$

$$= 1 + \frac{(3b^{I=1} + b^{I=0})}{F_K^2} \rho. \tag{54}$$

This extrapolation to the soft limit has been done without imposing the on-shell condition of the external particles. The expressions of Eqs. (44), (46), (48), and (51) have been obtained without taking the on-shell condition. Using this equation, the quark condensate can be estimated directly from the LECs determined from experiments within the linear density.

3.4.   *Coulomb correlation*
For the K^+p amplitude, we need to introduce the Coulomb correlation in order to compare it with the experimental data. Here we follow the prescription done in Refs. [24,25] originally

Table 1. Properties of the broad resonance states in the KN scattering with $S = +1$ and $I = 0$ around $\sqrt{s} = 1650$ MeV reported by Ref. [25]. The coupling strengths are obtained from the residue of the scattering amplitudes at the resonance positions (K. Aoki, private communication).

Solution	Resonance (J^P)	Mass [MeV]	Width [MeV]	Coupling strength [10^{-3} MeV^{-1}]
Solution 1	P_{01} ($\frac{1}{2}^+$)	1617	305	$5.26 - 2.62i$
Solution 2	P_{03} ($\frac{3}{2}^+$)	1678	463	$4.64 - 2.62i$

given in Ref. [31]. The Coulomb amplitude is calculated as

$$f_C = -\frac{\alpha}{2kv\sin^2(\theta/2)} \exp\left[-i\frac{\alpha}{v}\ln\left(\sin^2\frac{\theta}{2}\right)\right] \tag{55}$$

with the scattering angle θ, the fine structure constant α, and the K^+N relative velocity v defined by

$$v = \frac{k(E_K + E_p)}{E_K E_p}. \tag{56}$$

We add the Coulomb amplitude to the strong interaction amplitudes calculated by the chiral perturbation theory. In addition, we multiply the Coulomb phase shift factor $e^{2i\Phi_\ell}$ with

$$\Phi_\ell = \sum_{n=1}^{\ell} \tan^{-1}\frac{\alpha}{nv}, \tag{57}$$

for $\ell > 0$ ($\Phi_0 = 0$) to the strong interaction amplitudes. Finally, we have the amplitude with the Coulomb correlations as

$$f^{K^+p} = \sum_{\ell=0}^{\infty} \left[(\ell+1)T_{\ell+}^{I=1} + \ell T_{\ell-}^{I=1}\right]e^{2i\Phi_\ell}P_\ell(\cos\theta) - 8\pi\sqrt{s}f_C, \tag{58}$$

$$g^{K^+p} = \sum_{\ell=1}^{\infty}\left[T_{\ell+}^{I=1} - T_{\ell-}^{I=1}\right]e^{2i\Phi_\ell}\sin\theta\frac{dP_\ell(\cos\theta)}{d\cos\theta}. \tag{59}$$

3.5. *Inclusion of resonance state*

A recent work [25] proposed the presence of a broad resonance state in the KN scattering with $S = +1$ and $I = 0$ around $\sqrt{s} = 1650$ MeV. In Ref. [25], the authors paid close attention to a sudden increase of the $I = 0$ total cross section around $P_{\text{lab}} = 450$ MeV/c seen in the experimental data [32]. They constructed the K^+N scattering amplitudes using the chiral unitary approach and the model parameters were determined using observed cross sections of the K^+N elastic scattering up to $P_{\text{lab}} = 800$ MeV/c. They found the two best solutions for the K^+N amplitude with $I = 0$: in Solution 1 the P_{01} amplitude provides a dominant contribution, while in Solution 2 both P_{01} and P_{03} amplitudes contribute to the cross section. The former solution is more consistent with the Martin partial wave analysis [19]. Having performed analytic continuation of the obtained amplitudes into the complex energy plane, they found a resonance state in each solution. Solution 1 provides a resonance with 1617 MeV mass and 305 MeV width in the P_{01} partial wave, while Solution 2 finds the resonance with 1678 MeV mass and 463 MeV width in the P_{03} partial wave. The resonance parameters are summarized in Table 1. We will call the resonance in the former solution P_{01} resonance and the latter one P_{03} resonance in this paper.

The resonance energies correspond to $P_{\text{lab}} \sim 600$ MeV/c in the K^+N scattering. Since these resonances have a large width, the resonance may contribute to the $I = 0$ scattering amplitude

Table 2. Values of the physical constants that we use.

M_N	M_K	M_Λ	M_Σ	F_K	D	F
938.9 MeV	495.6 MeV	1115.7 MeV	1193.2 MeV	110.0 MeV	0.80	0.46

in a wide range of the energy around $P_{\text{lab}} \sim 600$ MeV/c. In addition, most of the low-energy data for the $I = 0$ cross section are in these energies. As the pole terms associated with reso-nances cannot be expressed in the perturbative expansion of energy, we take account of the resonance contribution explicitly in our amplitudes. The resonance state is introduced to the $I = 0$ amplitude by adding the following amplitude to the appropriate partial wave amplitude $T_{\ell = 1 \pm}$ defined in Eq. (40):

$$T^{\text{Pole}} = \frac{g^2 k^2}{\sqrt{s} - W + i\Gamma/2}, \tag{60}$$

where k is the c.m. momentum of the $K^+ N$ scattering, W and Γ are the mass and width of the resonance state, respectively, and g is the coupling strength of the resonance state to the $K^+ N$ $I = 0$ channel. The values of the coupling strengths are obtained as the residue of the scattering amplitudes at the resonance positions (K. Aoki, private communication).

4. Results

In this section, we show the numerical results of our calculations. First of all, we determine the values of the LECs appearing in the scattering amplitudes from the existing $K^+ N$ scattering data. We will see that the scattering amplitude for $I = 1$ is constrained well by the $K^+ p$ elastic scattering data, while the scattering amplitude with $I = 0$ is poorly determined due to the lack of data in particular for low energies and the large ambiguity of the $I = 0$ total cross section. Once the LECs are determined, we discuss the behavior of the quark condensate with strange quarks in the nuclear matter by using Eq. (54). We also discuss the in-medium quark condensates in hypothetical hyperonic matter in view of the flavor symmetry. In addition, we show our calculation of the wave function renormalization of the in-medium kaon. We use the isospin-averaged hadron masses as summarized in Table 2.

4.1. Determining LECs

We use the values of the low-energy constants in the leading order of the Lagrangian, D and F, given in Ref. [33], which are fixed by the hyperon semileptonic decays at tree level. The explicit values are shown in Table 2.

The values of the LECs for the NLO and NNLO, b^I, d^I, g^I, h^I, w^I for $I = 0, 1$ and $v_\pm$, given in Eqs. (49) and (53) are determined by carrying out the χ^2 fitting of the $K^+ N$ amplitude obtained by chiral perturbation theory to the experimental data. The reduced χ^2 function is defined as

$$\chi^2_{\text{d.o.f.}} = \frac{1}{\mathcal{N}_{\text{d.o.f.}}} \sum_i^n \left(\frac{y_i - f(x_i)}{\sigma_i} \right)^2, \tag{61}$$

where $y_i, f(x_i), \sigma_i$, and n are the experimental data, the theoretical calculations with the param-eters, the uncertainties of the data, and the number of data, respectively, and $\mathcal{N}_{\text{d.o.f.}}$ stands for the number of degrees of freedom defined as $\mathcal{N}_{\text{d.o.f.}} = n - m$ with the number of LECs $m = 12$. In our calculation, we consider partial waves up to the D-wave ($\ell = 2$) in the theoretical amplitudes. We will check the convergence of the partial wave decomposition. We restrict the

Table 3. Determined low-energy constants. FIT 1 uses Ref. [32] as the $I = 0$ total cross section, while FIT 2 employs Ref. [38]. Neither case introduces the broad resonance into the $I = 0$ amplitude. FIT 3 considers the P_{01} resonance by adding the resonance contribution, while FIT 4 takes account of the P_{03} resonance. In FIT 3 and FIT 4, Ref. [38] is used for the $I = 0$ total cross section.

LEC	Unit	FIT 1	FIT 2	FIT 3	FIT 4
$b^{I=1}$	[GeV^{-1}]	-1.07 ± 0.11	-1.10 ± 0.10	-0.11 ± 0.12	-1.08 ± 0.11
$d^{I=1}$	[GeV^{-1}]	-2.05 ± 0.20	-2.00 ± 0.17	-0.19 ± 0.19	-1.97 ± 0.17
$g^{I=1}$	[GeV^{-1}]	-0.82 ± 0.22	-0.93 ± 0.18	-0.80 ± 0.20	-1.01 ± 0.19
$h^{I=1}$	[GeV^{-1}]	3.67 ± 0.50	4.07 ± 0.60	0.91 ± 0.54	4.21 ± 0.60
$w^{I=1}$	[GeV^{-2}]	-0.76 ± 0.11	-1.00 ± 0.10	-0.36 ± 0.10	-1.05 ± 0.10
$b^{I=0}$	[GeV^{-1}]	-3.66 ± 0.30	1.45 ± 0.40	2.36 ± 0.48	2.29 ± 0.40
$d^{I=0}$	[GeV^{-1}]	-9.21 ± 0.40	-0.20 ± 0.40	-1.42 ± 0.58	-0.63 ± 0.50
$g^{I=0}$	[GeV^{-1}]	1.46 ± 0.50	6.10 ± 0.70	8.27 ± 0.95	8.07 ± 0.80
$h^{I=0}$	[GeV^{-1}]	16.29 ± 0.70	-3.99 ± 0.80	-1.64 ± 0.96	-4.91 ± 0.80
$w^{I=0}$	[GeV^{-2}]	-0.57 ± 0.29	4.23 ± 0.35	4.92 ± 0.46	4.99 ± 0.40
v_-	[GeV^{-1}]	42.89 ± 1.70	12.32 ± 1.70	5.00 ± 0.19	10.12 ± 1.70
v_+	[GeV^{-1}]	-7.55 ± 0.90	4.28 ± 0.90	-3.63 ± 0.93	4.74 ± 0.90
$\chi^2_{\text{d.o.f.}}$		2.41	2.74	2.95	2.96

energy region up to $P_{\text{lab}} = 800$ MeV/c, where inelastic contributions such as pion production start to be significant.

We determine all of the NLO and NNLO LECs simultaneously by using the experimental data of the $K^+ p$ differential cross section between $P_{\text{lab}} = 145$ and 726 MeV/c [34], the $K^+ n \to K^0 p$ charge exchange differential cross sections between $P_{\text{lab}} = 434$ and 780 MeV/c [35,36], the $I = 1$ total cross section between $P_{\text{lab}} = 145$ and 788 MeV/c [32,34,37–40], and the $I = 0$ total cross sections between $P_{\text{lab}} = 413$ and 794 MeV/c [32] and between $P_{\text{lab}} = 366$ and 714 MeV/c [38,40]. There are significant differences between the $I = 0$ total cross sections given in Refs. [32,38].

In this work, we consider four different fitting procedures for $I = 0$: FIT 1 uses Ref. [32] for the $I = 0$ total cross section, while FIT 2 employs Ref. [38]. Neither case introduces the broad resonance into the $I = 0$ amplitude. FIT 3 considers the P_{01} resonance by adding the resonance contribution (60) to the P_{01} scattering amplitude, while FIT 4 takes account of the P_{03} resonance. In FIT 3 and FIT 4, we use Ref. [38] for the $I = 0$ total cross section, because the resonance properties were obtained by using Bowen's results from Ref. [38] in Ref. [25]. In all four fittings, we do not use the differential cross sections of the $K^+ n$ elastic scattering due to their large experimental uncertainties.

The determined LECs for each case are summarized in Table 3. The table shows that the values of LECs for $I = 1$ in FITs 1, 2, and 4 are consistent with each other. We will see that the second best solution of FIT 3 is also consistent with these fits. This implies that the $K^+ p$ experimental data constrain the $I = 1$ KN amplitude very well.

In Figs. 1 and 2, we show our numerical results for the $I = 1$ total cross section and the $K^+ p$ elastic differential cross sections calculated with the determined LECs, respectively, and compare them with the experimental observations. For the total cross section in Fig. 1 we use the scattering amplitude calculated only with the strong interaction, while the $K^+ p$ differential cross sections in Fig. 2 include the Coulomb correlations formulated in Section 3.4. In both figures, four sets of the determined LECs reproduce the experimental observations very well in
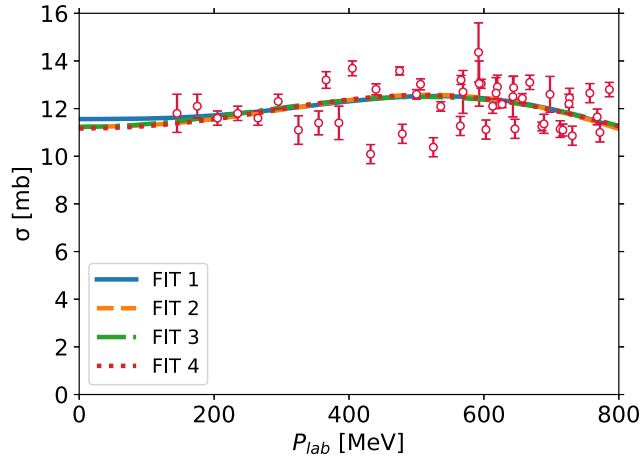
Fig. 1. $I = 1\ K^+N$ total cross sections calculated with the determined LECs given in Table 3 in comparison with the experimental data [32,34,37–40].

the same manner. It is notable that chiral perturbation theory works well to reproduce the $I = 1$ KN amplitude in the energy region that we consider. Some deviations among the four fittings become evident from $P_{\text{lab}} = 500\ \text{MeV}/c$ in the K^+p differential cross section.

In Figs. 3 and 4, we show the $I = 0$ total cross section and the differential cross sections for the charge exchange process $K^+n \rightarrow K^0p$ calculated with the determined LECs for each case, and we compare them with the experimental data. As stated above, for FIT 1 we use Ref. [32] for the data of the $I = 0$ total cross section, while in FITs 2, 3, and 4 Ref. [38] is used. Each fit reproduces the experimental data well. In particular, Fig. 4 shows that these four fits reproduce the experimental data well up to $P_{\text{lab}} = 720\ \text{MeV}/c$. Nevertheless, it should be emphasized that we find some deviations among the fits in the total cross sections at low energies below $300\ \text{MeV}/c$. This is because the LECs are not constrained so much in low energies due to the lack of experimental data. In fact, as seen in Table 3, the values of LECs for $I = 0$ are different in the fits. To fix the low-energy behavior of the scattering amplitude with $I = 0$, experimental data below $300\ \text{MeV}/c$ are extremely important. It is also interesting to mention that the total cross sections obtained by FIT 2 and FIT 4 are almost the same up to $600\ \text{MeV}/c$. In these fits, we use the same experimental data [38] but FIT 4 includes the P_{03} resonance contribution explicitly. Thus, our finding that FIT 2 and FIT 4 give a consistent result implies that the contribution of the P_{03} resonance can be absorbed into the LECs as discussed in Ref. [41]. This situation can be understood by the fact that the obtained LECs for FIT 2 and FIT 4 are also almost equivalent but there is a small deviation in the LECs for $I = 0$. These differences in the LECs represent the contribution of the P_{03} resonance.

In Fig. 5, we show the partial wave decomposition of the $I = 0$ total cross sections obtained by the four fitting procedures. As seen in the figure, each fit provides different contributions of the partial waves. In FITs 2, 3, and 4 the contribution of the D-wave is negligibly small. This shows that the partial wave decomposition works well up to the D-wave for these fits. In contrast, in FIT 1, the D-wave contribution is particularly large at higher momenta. Nevertheless, we find that the F-wave contribution is negligibly small in FIT 1 as shown in Fig. 5. This indicates again that the partial wave decomposition works well up to the F-wave in FIT 1. In FITs 2, 3, and 4, P-waves give essential contributions, while the S-wave contribution is found to be minor in all the fits, especially at low energies. In FIT 3, the contribution of the P_{01} partial wave is
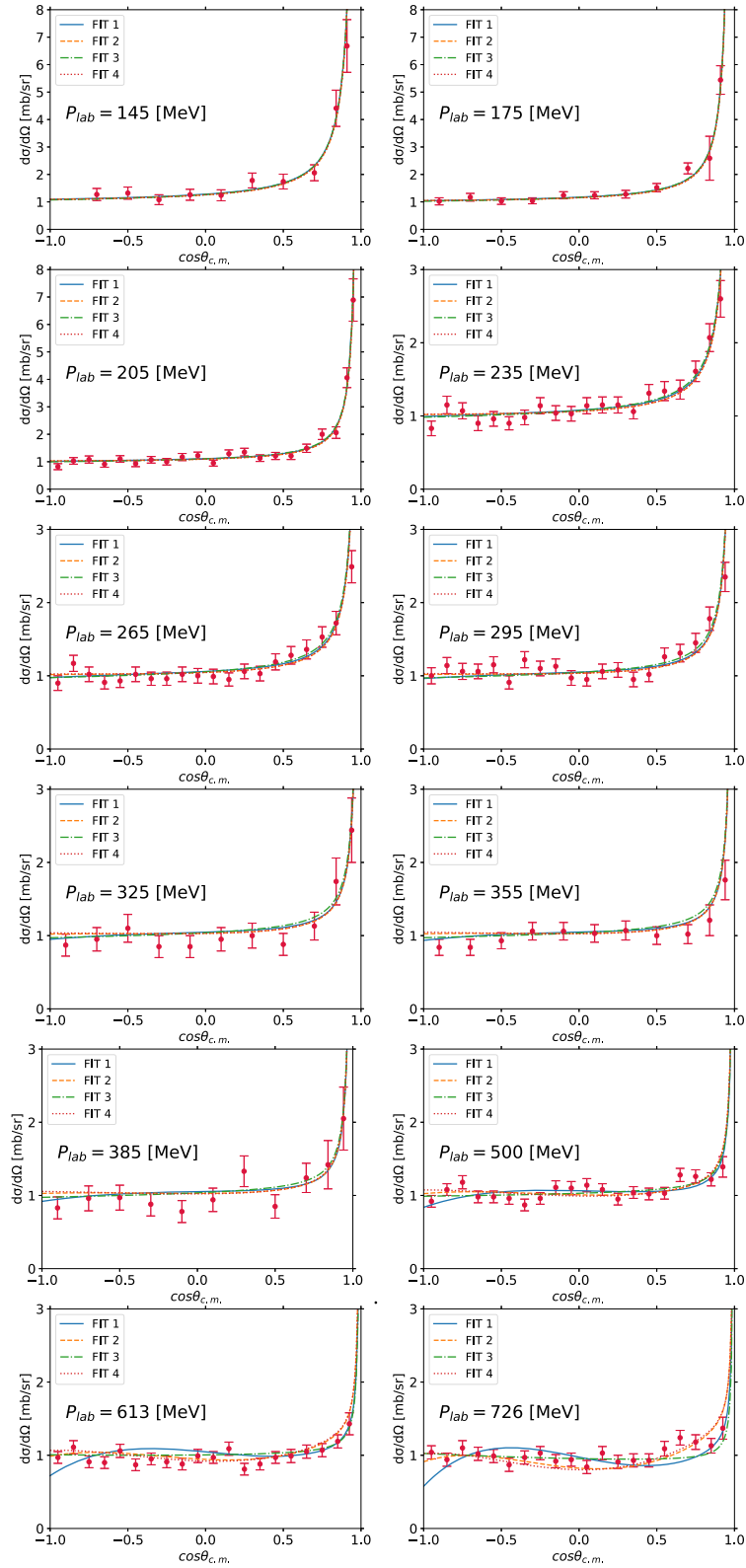
Fig. 2. Calculated differential cross sections of the K^+p elastic scattering in comparison with the experimental data of Ref. [34].
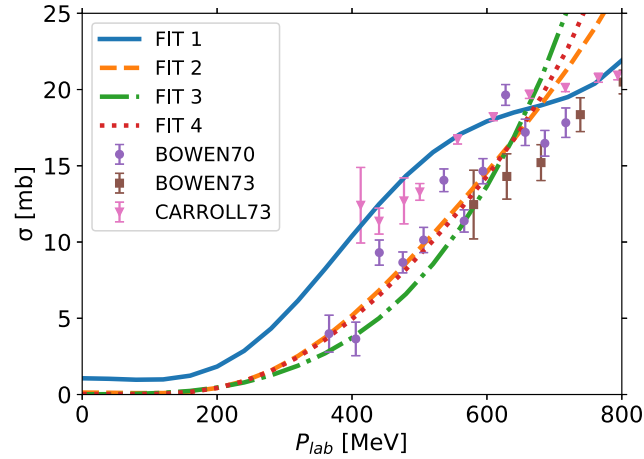
Fig. 3. $I = 0$ K^+N total cross sections calculated with the determined LECs given in Table 3 in comparison with the experimental data [32,38,40].

large, reflecting the explicit introduction of the resonance contribution into the amplitude. The partial wave decompositions of FITs 2 and 4 are also consistent each other. This tells us again that FITs 2 and 4 are almost equivalent.

In Fig. 6, we show our calculated results and the experimental data for the differential cross sections of the K^+n elastic scattering. Although the K^+n elastic scattering data are not used for the fitting, the K^+n elastic cross section should be reproduced according to the isospin symmetry, which is certainly good for hadronic reactions in these energies, because all of the theoretical calculations reproduce the cross sections of the K^+p elastic and $K^+n \to K^0p$ scatterings. Nevertheless, the experimental data are poorly reproduced at low energies and, in particular, for higher energies the theoretical predictions are scattered among the fittings. Figure 6 also shows that the difference between FIT 2 and FIT 4 can be seen at $\cos\theta_{\text{c.m.}} = 1$ for $P_{\text{lab}} > 680$ MeV/c, where the resonance contribution may be significant. This implies that forward scattering data for $P_{\text{lab}} > 680$ MeV/c may give us important constraints on the wide resonance with $S = +1$.

4.2. *Behavior of the in-medium quark condensate with strange quarks*

In this section, we discuss the behavior of the in-medium quark condensate with strange quarks by using Eq. (54) with the determined LECs in the previous section. It should be noted that we focus on the qualitative behavior of the quark condensate in nuclear matter, because the condensate (54) is calculated under the linear density approximation. In addition, to separate out $\langle \bar{s}s \rangle^*$ from Eq. (54) one needs to calculate the in-vacuum condensates taking into account the SU(3) breaking effect. We also note that, as we have seen in the previous section that the LECs are not determined well with the existing data, a discussion on the detailed value of the in-medium quark condensate is not within the scope of this paper.

As seen in Eq. (54), the sign of the coefficient of the linear density, $3b^{I=1} + b^{I=0}$, determines whether the condensate increases or decreases in the nuclear matter. The slope parameters obtained in the present calculation are summarized in Table 4. There the central values of the determined LECs are used. The table shows that the determined slope parameters are mostly negative, which means that the magnitude of the quark condensate decreases as the density increases, but their values differ in a wide range. For comparison, we also show the values of the slope parameters evaluated by the LECs determined in other calculations based on the
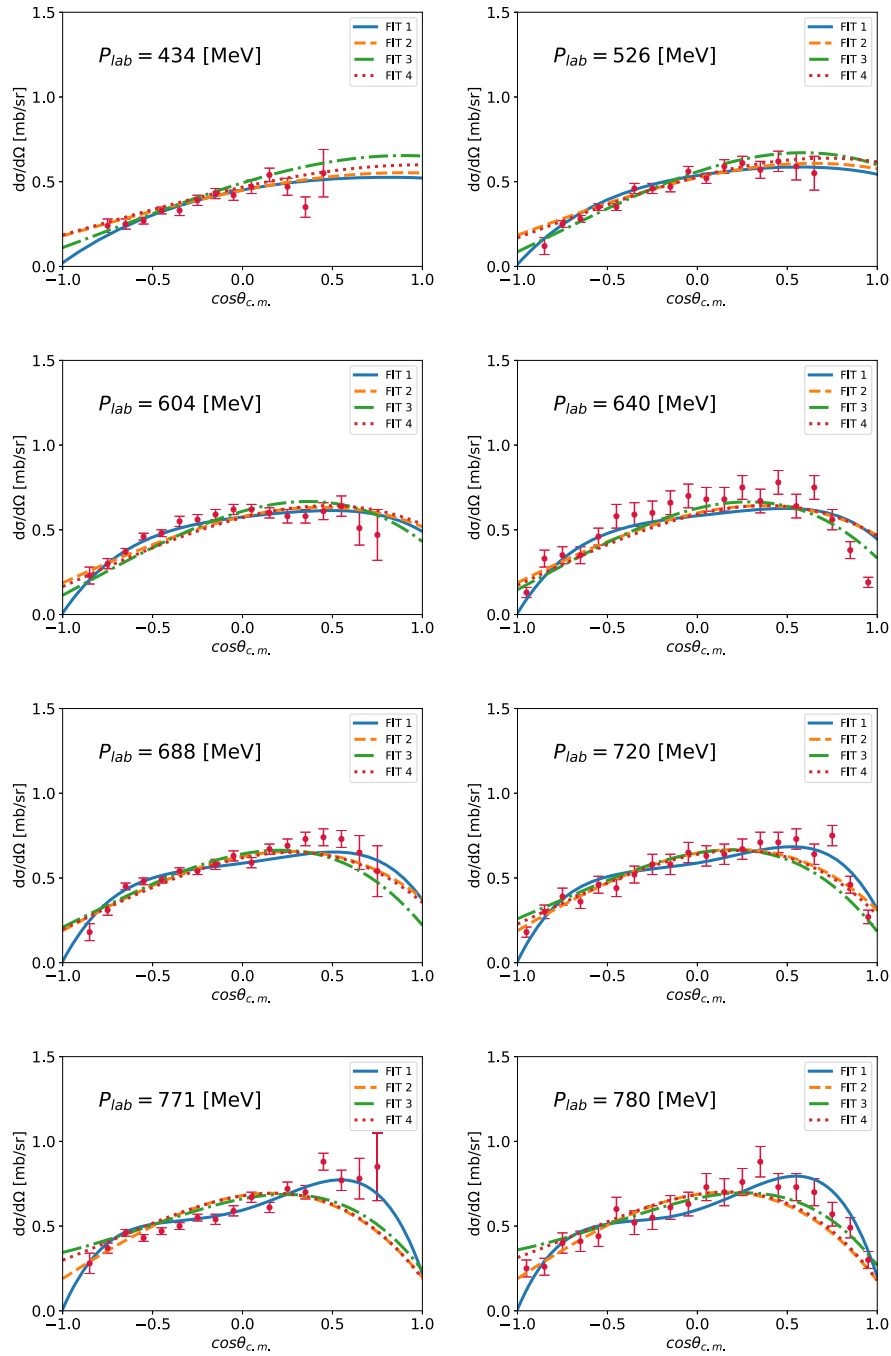
Fig. 4. Calculated differential cross sections of $K^+n \to K^0p$ charge exchange scattering in comparison with the experimental data of Refs. [35,36]. The data for the momenta at $P_{\text{lab}} = 640$, 720, and 780 MeV/c are taken from Ref. [35], the others from Ref. [36].

baryon masses. As a theoretical calculation, we use the LECs determined by lattice calculation. Reference [30] expressed the octet baryon masses in terms of the LECs by using an $\mathcal{O}(p^4)$ chiral perturbation theory in the extended-on-mass-shell scheme and determined the LECs by fitting them to lattice QCD calculation with various values of the quark masses. In addition, we also consider the LECs in more phenomenological determinations. The values of b_F and b_D can be fixed by the mass splitting of the octet baryons in the leading order of chiral perturbation the-
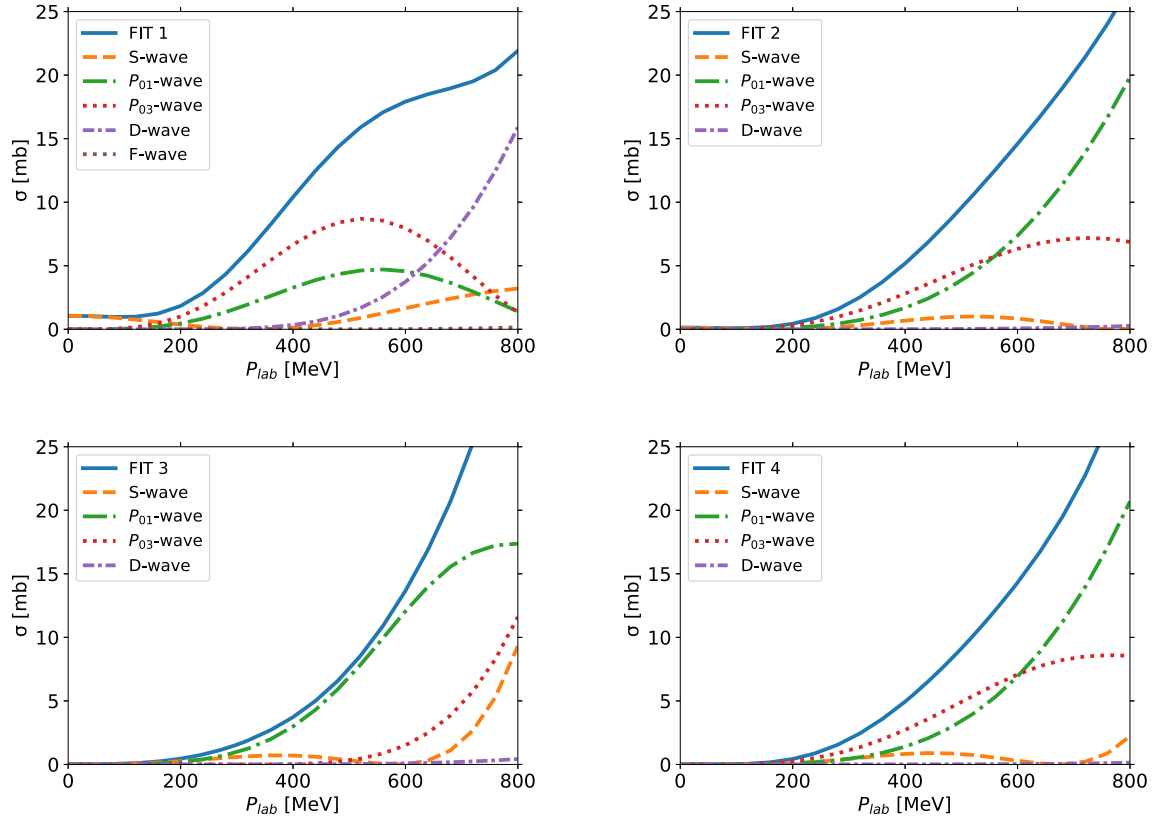
Fig. 5. Partial wave contributions of the $I = 0$ K^+N total cross section calculated with the determined LECs.

Table 4. Values of the slope parameter ($3b^{I=1} + b^{I=0}$) appearing in Eq. (54) obtained in the present work. The central values of the determined LECs are used. FIT 3′ is the second best solution of the fitting procedure FIT 3. The values of the slope parameters calculated with the LECs in other calculations, a theoretical calculation using lattice data [30], a phenomenological calculation using the octet baryon masses [42,43] together with the $\sigma_{\pi N}$ term (see text), and a global fitting of LECs in chiral perturbation theory using πN and KN phase shift analyses [45], are also shown. These works are referred as Th., Pheno. and ChPT, respectively. The values of the relevant LECs for these calculations are $(b_0, b_D, b_F) = (-0.609, 0.225, -0.404)$, $(-0.711, 0.060, -0.190)$ and $(b^{I=0}, b^{I=1}) = (0.136, -0.270)$, respectively.

[GeV^{-1}]	FIT 1	FIT 2	FIT 3	FIT 4	FIT 3′	Th.	Pheno.	ChPT
$3b^{I=1} + b^{I=0}$	-6.87	-1.86	2.02	-0.96	-1.98	-1.36	-2.47	-0.674

ory as given, for instance, in Refs. [42,43], while we fix the value of b_0 by the $\sigma_{\pi N}$ term together with b_F and b_D using the relation between the LECs of the SU(2) and SU(3) chiral perturbation theories given in Ref. [15] as

$$2b_0 + b_D + b_F = 2b_0 + b^{I=1} - b^{I=0} = 2c_1 \qquad (62)$$

where c_1 is one of the SU(2) LECs and is given by $c_1 = -\sigma_{\pi N}/(4m_\pi^2)$ in the leading order of chiral perturbation theory. Its value can be fixed as $c_1 = -0.78\,\text{GeV}^{-1}$ by using $\sigma_{\pi N} = 60\,\text{MeV}$, as suggested recently in Refs. [8–12]. This value is also consistent with a recent analysis based on pionic atom data [44]. With this value, however, the linear density approximation provides as much as 50% reduction of the quark condensate in magnitude at the saturation density, while a smaller value, $\sigma_{\pi N} \simeq 45\,\text{MeV}$, is preferable to reproduce 35% reduction in the linear density
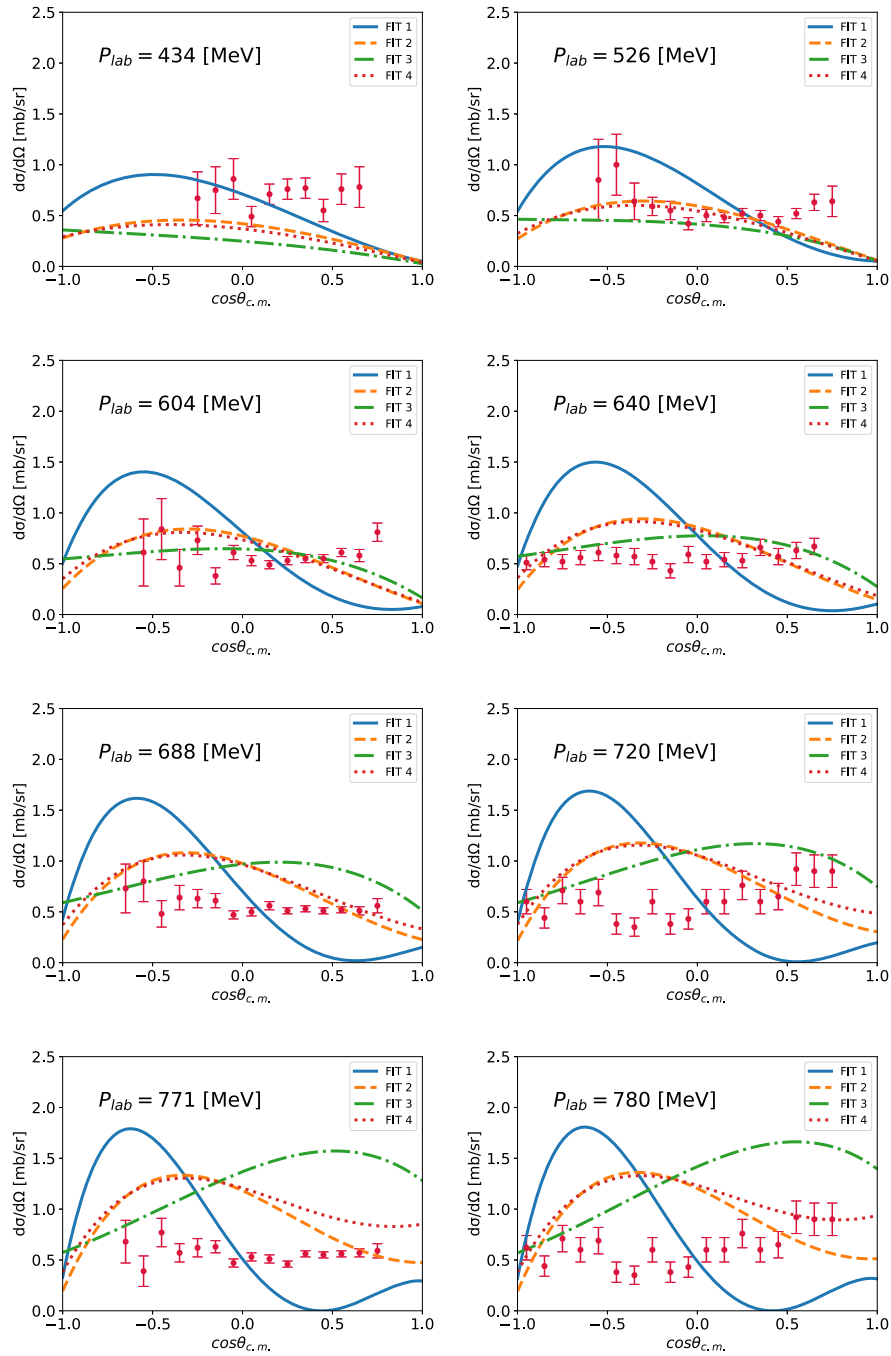
Fig. 6. Calculated differential cross sections of K^+n elastic scattering in comparison with the experimental data of Refs. [35,36]. The data for the momenta at $P_{\text{lab}} = 640$, 720, and 780 MeV/c are taken from Ref. [35], the others from Ref. [36].

analysis. In any case, it is a good advantage of the present work that the slope parameter is directly determined by the physical observables without using the value of the $\sigma_{\pi N}$ term. In addition, we also compare the LECs obtained by a global fitting performed in Ref. [45]. There the πN and KN scattering amplitudes were calculated using chiral perturbation theory up to $\mathcal{O}(p^3)$ for the πN channel and $\mathcal{O}(p^2)$ for the KN channel. (They also performed calculations with KN amplitudes including one-loop contributions, which are part of $\mathcal{O}(p^3)$). The LECs
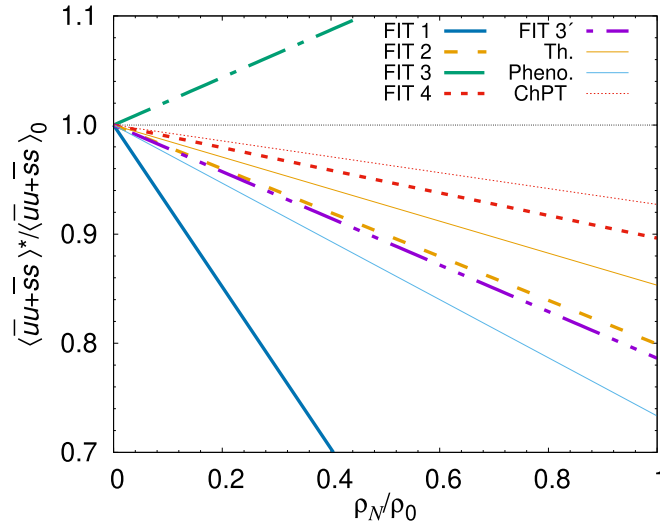
Fig. 7. Density dependence of the in-medium quark condensate with strange quarks normalized by the in-vacuum condensate calculated with the slope parameters given in Table 4. We use $\rho_0 = 0.17 \, \text{fm}^{-3}$.

were determined commonly by using πN and KN phase shift analyses. For the KN scattering they used the SP92 solution [22] and took the KN phase shifts only at low energies between $P_{\text{lab}} = 25$ and $257 \, \text{MeV}/c$. Note that our study uses direct scattering data in a much wider range up to $800 \, \text{MeV}/c$, where the scattering data are available from $P_{\text{lab}} = 145 \, \text{MeV}/c$ for the $K^+ p$ channel and from $434 \, \text{MeV}/c$ for the $K^+ n$ channel. In Table 4, we show the LECs obtained by the fitting strategy in Ref. [45] where they did not consider the constraint on the LECs from the baryon masses.

In Fig. 7, we show the density dependence of the in-medium quark condensate with strange quarks normalized by the in-vacuum condensate. The calculation is done with Eq. (54) using the slope parameters shown in Table 4. The behavior of the in-medium condensate is highly dependent on the choice of the parameter sets. The quark condensates with FITs 2 and 4 decrease in magnitude moderately as the density increases and the reduction at the saturation density ρ_0 is found to be about 10–20%. The baryon mass determinations of the LECs also give consistent results. The quark condensate calculated with FIT 1 decreases significantly and moves out of the range of reliability. This implies that the current status of the $K^+ N$ scattering data may not be of sufficient quality for the determination of the LECs.

In contrast to the findings with FITs 1, 2, and 4, the quark condensate calculated with FIT 3 largely increases in magnitude. This behavior might be unnatural in the context of the partial restoration of DBχS in finite density. For FIT 3, which uses Ref. [38] for the $I = 0$ total cross section and introduces the P_{01} broad resonance, we find the second best solution that minimizes Eq. (61). This solution is named FIT 3' and its LECs are shown in Table 5. Comparing the LECs for $I = 1$ of FIT 3' with those of the other fits, we find that FIT 3' has LECs closer to FITs 1, 2, and 4. The results of the calculations of the slope parameter and the in-medium quark condensate using the LEC of FIT 3' are also shown in Table 4 and Fig. 7, respectively, which show that the density dependence of the quark condensate for FIT 3' is consistent with FITs 2 and 4. The existence of a more reasonable solution with a similar $\chi^2_{\text{d.o.f.}}$ value does not imply that the fitting procedure 3, where we have assumed a P_{01} resonance, should be immediately ruled out. The fact that there is another independent solution to minimize $\chi^2_{\text{d.o.f.}}$ with a similar

Table 5. Same as FIT 3 in Table 3 but showing LECs for the second best solution.

LEC	Unit	FIT 3$'$
$b^{I=1}$	[GeV^{-1}]	-0.39 ± 0.12
$d^{I=1}$	[GeV^{-1}]	-0.69 ± 0.18
$g^{I=1}$	[GeV^{-1}]	-1.07 ± 0.21
$h^{I=1}$	[GeV^{-1}]	2.07 ± 0.50
$w^{I=1}$	[GeV^{-2}]	-0.66 ± 0.10
$b^{I=0}$	[GeV^{-1}]	-0.82 ± 0.50
$d^{I=0}$	[GeV^{-1}]	-1.95 ± 0.60
$g^{I=0}$	[GeV^{-1}]	1.03 ± 0.90
$h^{I=0}$	[GeV^{-1}]	3.91 ± 0.90
$w^{I=0}$	[GeV^{-2}]	-0.11 ± 0.40
v_-	[GeV^{-1}]	6.89 ± 0.19
v_+	[GeV^{-1}]	-1.98 ± 0.90
$\chi^2_{\text{d.o.f.}}$		3.00

value may indicate that the LECs giving the smallest value of $\chi^2_{\text{d.o.f.}}$ can be changed for more experimental observations in the future, such as the K^+d reaction at J-PARC [46] and the $K^0 p$ reaction at the K-Long Facility at Jefferson Laboratory [47].

The choice of the experimental data of the $I=0$ total cross sections and the presence or absence of the resonance state in $I=0$ K^+N scattering have a significant impact on the determination of the LECs. Therefore, we emphasize that, in order to determine the behavior of the in-medium quark condensate with strange quarks more precisely, it is extremely important to determine experimental values accurately and consistently with isospin symmetry at a wide range of energy, in particular much lower than $P_{\text{lab}} = 600\,\text{MeV}/c$, where the effects of the resonance state are less significant.

4.3. *Quark condensate in SU(3) symmetric baryonic matter*

In the previous section, we have discussed the quark condensate including the strange quark component in symmetric nuclear matter. This is an SU(3) flavor extension of the quark condensate in nuclear matter. From the flavor symmetry point of view, it is also interesting to consider the SU(3) flavor extension of the matter. Nuclear matter consists of nucleons without explicit strange content. In this sense, we discuss an SU(3) quark condensate in the SU(2) symmetric baryonic matter. It may also be interesting to extend the discussion on the quark condensates in nuclear matter further to those in hypothetical hyperonic matter in order to discuss them from the viewpoint of flavor SU(3) symmetry. This kind of analysis might be interesting if one considers the explicit SU(3) breaking on the quark masses and the hadronic quantities such as the decay constants and masses. If one traces the SU(3) breaking effects on the in-medium quark condensate, the nuclear matter itself can also be a source of SU(3) breaking. Note, however, that while the quark condensates in nuclear matter can be studied phenomenologically by the properties of the Nambu–Goldstone bosons in atomic nuclei as has been done in pionic atoms and pion–nucleus scattering, the quark condensate in hyperonic matter would be rather academic due to the absence of hyperon matter in laboratories.

Just as symmetric nuclear matter consists of the same number of protons and neutrons, we define SU(3) symmetric baryonic matter so as to consist of the same number of octet baryons with $J^p = 1/2^+$, p, n, Λ, Σ^+, Σ^0, Σ^-, Ξ^0, and Ξ^-. We further consider Λ-hyperonic matter, containing only the Λ hyperon; Σ-hyperonic matter, which has the same number of Σ^+, Σ^0, and Σ^-; and Ξ-hyperonic matter, which consists of the same numbers of Ξ^0 and Ξ^-.

The light quark condensate $\langle \bar{u}u + \bar{d}d \rangle$ in nuclear and hyperonic matter can be calculated in the same way as in Section 2 and is expressed in the linear density approximation by the isospin-averaged scattering amplitude of the pion and the corresponding baryon in the soft limit as in Eq. (15). The pion scattering amplitudes are calculated by chiral perturbation theory and expressed by LECs. The scattering amplitudes relevant to the current calculation are shown in Appendix A. Taking the soft limit of the scattering amplitude, we obtain the quark condensate $\langle \bar{u}u + \bar{d}d \rangle$ in nuclear and hyperonic matter as

$$\frac{\langle \bar{u}u + \bar{d}d \rangle_N^*}{\langle \bar{u}u + \bar{d}d \rangle_0} = 1 + \frac{4b_0 + 2b_D + 2b_F}{F_\pi^2} \rho_B, \tag{63a}$$

$$\frac{\langle \bar{u}u + \bar{d}d \rangle_\Lambda^*}{\langle \bar{u}u + \bar{d}d \rangle_0} = 1 + \frac{4b_0 + \frac{4}{3}b_D}{F_\pi^2} \rho_B, \tag{63b}$$

$$\frac{\langle \bar{u}u + \bar{d}d \rangle_\Sigma^*}{\langle \bar{u}u + \bar{d}d \rangle_0} = 1 + \frac{4b_0 + 4b_D}{F_\pi^2} \rho_B, \tag{63c}$$

$$\frac{\langle \bar{u}u + \bar{d}d \rangle_\Xi^*}{\langle \bar{u}u + \bar{d}d \rangle_0} = 1 + \frac{4b_0 + 2b_D - 2b_F}{F_\pi^2} \rho_B, \tag{63d}$$

where ρ_B is the density of the baryon number in each baryonic matter, and we write these expressions in terms of the original LECs appearing in the Lagrangian in order to make the SU(3) flavor structure clear. The relations to the LECs $b^{I=1}$ and $b^{I=0}$ are given in Eq. (49a). Similarly, the quark condensate $\langle \bar{u}u + \bar{s}s \rangle$ in hyperonic matter is obtained by the soft limit of the isospin-averaged kaon–hyperon scattering amplitude in the linear density approximation and expressed by the LECs as

$$\frac{\langle \bar{u}u + \bar{s}s \rangle_N^*}{\langle \bar{u}u + \bar{s}s \rangle_0} = 1 + \frac{4b_0 + 3b_D - b_F}{F_K^2} \rho_B, \tag{64a}$$

$$\frac{\langle \bar{u}u + \bar{s}s \rangle_\Lambda^*}{\langle \bar{u}u + \bar{s}s \rangle_0} = 1 + \frac{4b_0 + \frac{10}{3}b_D}{F_K^2} \rho_B, \tag{64b}$$

$$\frac{\langle \bar{u}u + \bar{s}s \rangle_\Sigma^*}{\langle \bar{u}u + \bar{s}s \rangle_0} = 1 + \frac{4b_0 + 2b_D}{F_K^2} \rho_B, \tag{64c}$$

$$\frac{\langle \bar{u}u + \bar{s}s \rangle_\Xi^*}{\langle \bar{u}u + \bar{s}s \rangle_0} = 1 + \frac{4b_0 + 3b_D + b_F}{F_K^2} \rho_B. \tag{64d}$$

The quark condensates in the SU(3) symmetric baryonic matter are also obtained as:

$$\frac{\langle \bar{u}u + \bar{d}d \rangle_B^*}{\langle \bar{u}u + \bar{d}d \rangle_0} = \frac{1}{8} \left[2 \frac{\langle \bar{u}u + \bar{d}d \rangle_N^*}{\langle \bar{u}u + \bar{d}d \rangle_0} + \frac{\langle \bar{u}u + \bar{d}d \rangle_\Lambda^*}{\langle \bar{u}u + \bar{d}d \rangle_0} + 3 \frac{\langle \bar{u}u + \bar{d}d \rangle_\Sigma^*}{\langle \bar{u}u + \bar{d}d \rangle_0} + 2 \frac{\langle \bar{u}u + \bar{d}d \rangle_\Xi^*}{\langle \bar{u}u + \bar{d}d \rangle_0} \right]$$

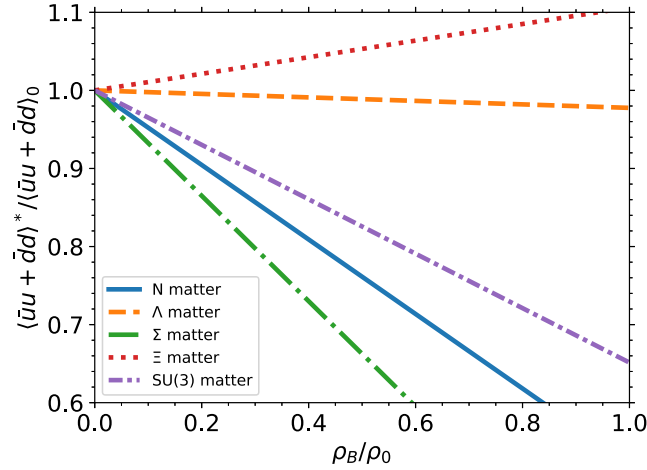$$= 1 + \frac{4b_0 + \frac{8}{3}b_D}{F_\pi^2} \rho_B, \tag{65}$$

Fig. 8. Baryon density dependence of $\langle \bar{u}u + \bar{d}d \rangle$ in nuclear matter, hyperonic matter, and the SU(3) symmetric baryonic matter. The LECs of FIT 2 are used and b_0 is fixed by Eq. (62) with $c_1 = -0.78$ GeV^{-1}. We use $F_\pi = 93$ MeV and $\rho_0 = 0.17$ fm^{-3}.

$$\frac{\langle \bar{u}u + \bar{s}s \rangle_B^*}{\langle \bar{u}u + \bar{s}s \rangle_0} = \frac{1}{8} \left[2 \frac{\langle \bar{u}u + \bar{s}s \rangle_N^*}{\langle \bar{u}u + \bar{s}s \rangle_0} + \frac{\langle \bar{u}u + \bar{s}s \rangle_\Lambda^*}{\langle \bar{u}u + \bar{s}s \rangle_0} + 3 \frac{\langle \bar{u}u + \bar{s}s \rangle_\Sigma^*}{\langle \bar{u}u + \bar{s}s \rangle_0} + 2 \frac{\langle \bar{u}u + \bar{s}s \rangle_\Xi^*}{\langle \bar{u}u + \bar{s}s \rangle_0} \right]$$

$$= 1 + \frac{4b_0 + \frac{8}{3}b_D}{F_K^2} \rho_B. \tag{66}$$

The SU(3) quark condensate in the SU(3) symmetric baryonic matter is calculated as

$$\frac{\langle \bar{u}u + \bar{d}d + \bar{s}s \rangle_B^*}{\langle \bar{u}u + \bar{d}d + \bar{s}s \rangle_0} = \frac{2}{3} \left(\frac{\langle \bar{u}u + \bar{s}s \rangle_B^*}{\langle \bar{u}u + \bar{s}s \rangle_0} + \frac{1}{2} \frac{\langle \bar{u}u + \bar{d}d \rangle_B^*}{\langle \bar{u}u + \bar{d}d \rangle_0} \right) = 1 + \frac{4b_0 + \frac{8}{3}b_D}{F^2} \rho_B, \tag{67}$$

where we assume flavor symmetry for the in-vacuum condensates $\langle \bar{u}u \rangle_0 = \langle \bar{d}d \rangle_0 = \langle \bar{s}s \rangle_0$ and the meson decay constants $F = F_\pi = F_K$. As one expects, the slope parameters of Eqs. (63), (65), and (67) should be equivalent according to the flavor symmetry because the matter is flavor-symmetric.

As we have seen in the previous section, to evaluate the quark condensate $\langle \bar{u}u + \bar{s}s \rangle$ in the nuclear matter, we just need the two parameters $b^{I=1}$ and $b^{I=0}$, which can be fixed by the K^+N scattering. On the other hand, for other cases we need to know the value of b_0. Here we determine it by Eq. (62) with $c_1 = -0.78$ GeV^{-1}. In the following we use the LECs $b^{I=1}$ and $b^{I=0}$ determined in FIT 2 as an example.

Firstly, we plot the behavior of $\langle \bar{u}u + \bar{d}d \rangle$ in nuclear matter, hyperon matter, and the SU(3) symmetric baryonic matter in Fig. 8. This figure shows the SU(3) flavor symmetry breaking for the baryonic matter since the condensate $\langle \bar{u}u + \bar{d}d \rangle$ has no strange components but the hyperonic matter contains strange quarks. The relative amount of up and down quarks in the hyperonic matter is less than in nuclear matter, so the condensate in the hyperonic matter is expected to decrease less than that in nuclear matter. Figure 8 shows that the quark condensates in Λ-matter and Ξ-matter increase in magnitude, while the quark condensate in Σ-hyperonic matter decreases more than that in nuclear matter. On the other hand, the condensate in the SU(3) symmetric baryonic matter is reduced but not more than that in nuclear matter; this is an expected behavior.
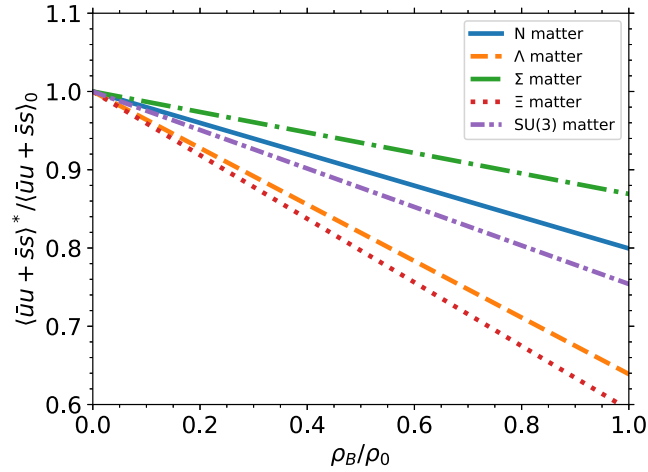
Fig. 9. Same as Fig. 8, but for $\langle \bar{u}u + \bar{s}s \rangle$.

Next, we plot the density dependence of $\langle \bar{u}u + \bar{s}s \rangle$ in nuclear matter, hyperonic matter, and the SU(3) symmetric baryonic matter in Fig. 9. The calculation shows that the quark condensates $\langle \bar{u}u + \bar{s}s \rangle$ in Λ-hyperonic matter and Ξ-hyperonic matter are reduced compared to the quark condensate in nuclear matter, but the condensate in Σ-matter is reduced less than that in nuclear matter. Thus, since hyperonic matter contains strange quarks, one expects that the quark condensate with strange components in hyperonic matter would be reduced compared to the quark condensate in nuclear matter, but this is not necessarily the case. On the other hand, the condensate in the SU(3) symmetric baryonic matter is reduced compared to that in nuclear matter; this is also an expected behavior.

4.4.   *Wave function renormalization of the in-medium kaon*

The wave function renormalization of the NG bosons in the nuclear medium has been investigated as one of the important in-medium modifications of the hadron properties, for instance, in Refs. [3,4,24,48–51]. References [48,49] pointed out that the pion wave function renormalization in the nuclear medium is responsible for the in-medium change of the pion decay constant. In Ref. [3], the wave function renormalization for the in-medium pion was discussed to explain the missing repulsion of the in-medium πN scattering length. Reference [24] calculated the wave function renormalization for the in-medium kaon using the K^+N amplitude described by chiral dynamics and found that the leading-order analysis with the Weinberg–Tomozawa interaction suggested 8% enhancement of the wave function normalization factor at normal nuclear density, and full calculations provided about 2–6% enhancement depending on the kaon momentum. This indicates that the K^+N interaction may be enhanced about several percent in nuclear matter. This is partially consistent with the phenomenological finding of the enhancement of the K^+N elastic scattering amplitude in the nucleus [37,52–55].

Here we update the study of Ref. [24] by using the K^+N scattering amplitudes constructed using more general terms in chiral perturbation theory and determined by wider fitting procedures. According to Ref. [24], the wave function renormalization factor Z_K for the in-medium kaon is obtained by using the optical potential for a kaon in nuclear matter V_{opt} as

$$Z_K \equiv 1 + \frac{M_K}{\omega_K} \left. \frac{\partial V_{\text{opt}}}{\partial \omega_K^*} \right|_{\omega_K^* = \omega_K}, \tag{68}$$
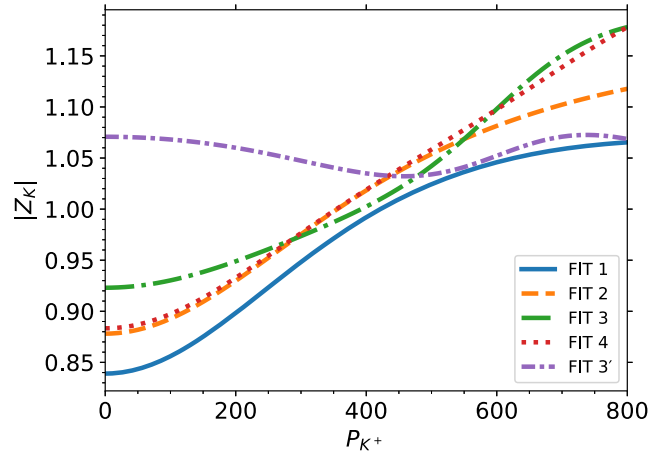
Fig. 10. Momentum dependence of the absolute value of the wave function renormalization factor Z_K for the kaon at normal nuclear density.
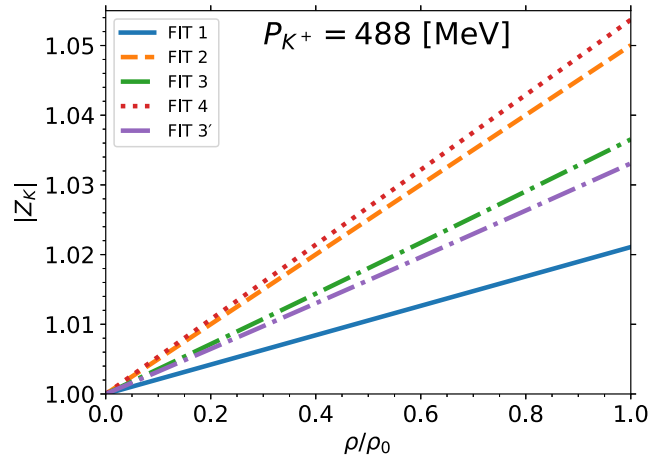

Fig. 11. Density dependence of the absolute value of the wave function renormalization factor Z_K at $P_{K^+} = 488$ MeV/c.

where ω_K is the kaon energy. In the linear density approximation the optical potential is given by the KN scattering amplitude as

$$2M_K V_{\text{opt}}(\omega_K) = \frac{\rho}{2M_N} T_{KN}(\omega_K). \qquad (69)$$

We calculate the wave function renormalization for the in-medium kaon using the K^+N scattering amplitudes constructed in the previous section.

The wave function renormalization factor Z_K at normal nuclear density is shown in Fig. 10 as a function of the momentum of kaon in nuclear matter P_{K^+}. We find in the figure that the momentum dependences of wave function renormalization factors obtained by FITs 1 to 4 are qualitatively consistent with each other and monotonically increase with respect to P_{K^+}, while Z_K with FIT 3$'$ is almost independent of P_{K^+} and gives almost 6% enhancement. We show the linear density dependence of the wave function renormalization factor Z_K at $P_{K^+} = 488$ MeV/c in Fig. 11. The enhancement of the wave function renormalization factors is found to be around 2–5% depending on the fitting procedures. This result is consistent with the previous study. In the case of the in-medium pion, the wave function renormalization factor is enhanced by 40%

at normal nuclear density [50]. Compared to the case of the in-medium pion, our calculation gives a smaller enhancement at normal nuclear density.

5.   Summary

We have investigated the $K^+ N$ scattering amplitude using chiral perturbation theory in order to estimate the in-medium quark condensate with strange quarks. The in-medium quark condensate is calculated based on the correlation function approach. There the in-medium quark condensate with strange quarks is given by the correlation function of the pseudoscalar fields with the kaon quantum number in nuclear matter at the soft limit. In the linear density approximation, the in-medium correlation function is reduced to the product of the KN scattering amplitude and the nuclear density. We utilize chiral perturbation theory to describe the KN scattering amplitude. It is good that the amplitude in chiral perturbation theory is described by an analytic function and can be analytically continued to the soft limit.

   We have determined the low-energy constants (LECs) of the SU(3) chiral perturbation theory appearing in the KN scattering amplitude by the existing scattering data. The scattering amplitudes have been calculated up to the next-to-leading order in chiral perturbation theory and in addition we have also included the strange quark mass-dependent terms of the next-to-next-to-leading order in order to improve extrapolation to the strange sector. The LECs appearing here characterize the interaction between K^+ and N. We have performed several fitting procedures for the LECs using the experimental data of the $K^+ p$ differential cross section, the $K^+ n \to K^0 p$ charge exchange differential cross sections, and $I = 1$ and $I = 0$ total cross sections. For the experimental data of the $I = 0$ total cross section, we take two choices because two data sets look inconsistent. In addition, we have further choices to include a broad resonance state with $I = 0$ around $P_{\text{lab}} = 600\,\text{MeV}/c$, which was proposed in Ref. [24], or not. We have obtained such a nice amplitude for $I = 1$ that it reproduces the experimental data below $P_{\text{lab}} = 800\,\text{MeV}$ almost perfectly. For the $I = 0$ amplitude, we have used the $I = 0$ total cross section and the differential cross section of the $K^+ n \to K^0 p$ to determine the LECs in the $I = 0$ amplitude. We have found that the scattering data for $I = 0$ are also reproduced well but the LECs are not uniquely determined and depend on the fitting procedures. In addition it has turned out that the differential cross section of the $K^+ n$ elastic scattering are not reproduced even though the isospin symmetry should fix the $K^+ n$ amplitude from the $K^+ p \to K^+ p$ and $K^+ n \to K^0 p$ amplitudes.

   With the determined LECs, we have discussed the behavior of the in-medium quark condensate with strange components in the linear density approximation. We have found that the slope parameter of the linear density is dependent on the fitting procedures. This implies that the current $K^+ N$ experiment data, especially at low energies, do not have enough accuracy to fix the LECs. Some parameter sets provide consistent results of the slope parameter with other determinations of the LECs such as those based on the baryon masses in lattice calculations for various quark masses. We have also calculated the quark condensates, $\langle \bar{u}u + \bar{d}d \rangle$ and $\langle \bar{u}u + \bar{s}s \rangle$, in hyperonic matter and the SU(3) symmetric baryonic matter from the viewpoint of flavor symmetry. Moreover, we have calculated $\langle \bar{u}u + \bar{d}d + \bar{s}s \rangle$ in the SU(3) symmetric baryonic matter and obtained a 25% restoration of the chiral symmetry in the case of SU(3) with our fitted LECs. This result is consistent with the case of the SU(2) condensate in nuclear matter. We have calculated the wave function renormalization factor using the obtained T-matrix of KN. In any FITs, the wave function renormalization factor for the in-medium kaon with an intermediate

momentum such as $P_{K^+} = 488$ MeV/c increases as the density increases, but the enhancement is not as large as that for the in-medium pion.

In conclusion, thanks to good accuracy and the wide range of the K^+p elastic scattering data, the KN scattering amplitude with $I = 1$ is well controlled in chiral perturbation theory. With this success, the correlation function approach with the linear density approximation has worked well to see qualitative features of the in-medium strange quark condensate. Nevertheless, we emphasize that, in order to determine the behavior of the in-medium quark condensate with strange quarks more accurately, it is important to determine the K^+N scattering amplitudes at energies much lower than $P_{\text{lab}} = 400$ MeV/c, where the amplitude may be free from the effect of the possible resonance state.

A. Meson–baryon scattering *T*-matrices for the quark condensates

In this section, we give a list of meson–baryon scattering T-matrices relevant to the calculation of in-medium quark condensates. As seen in Eq. (15), we need the T-matrices of the meson–baryon scattering in the soft limit. As discussed in Section 3.3, the terms in the T-matrix relevant to the quark condensate are the terms involving the LECs b_0, b_D, and b_F, which appear in the next-to-leading order of the chiral Lagrangian (22).

For evaluation of the in-medium condensate $\langle \bar{u}u + \bar{d}d \rangle$, we use the T-matrices of the pion–baryon:

$$T_{\pi^0 p} = \frac{2B_0 m (4b_0 + 2b_D + 2b_F)}{F_\pi^2} \times 2M_N, \tag{A1a}$$

$$T_{\pi^0 n} = \frac{2B_0 m (4b_0 + 2b_D + 2b_F)}{F_\pi^2} \times 2M_N, \tag{A1b}$$

$$T_{\pi^0 \Lambda} = \frac{2B_0 m \left(4b_0 + \frac{4}{3}b_D\right)}{F_\pi^2} \times 2M_\Lambda, \tag{A1c}$$

$$T_{\pi^0 \Sigma^+} = \frac{2B_0 m (4b_0 + 4b_D)}{F_\pi^2} \times 2M_\Sigma, \tag{A1d}$$

$$T_{\pi^0 \Sigma^-} = \frac{2B_0 m (4b_0 + 4b_D)}{F_\pi^2} \times 2M_\Sigma, \tag{A1e}$$

$$T_{\pi^0 \Sigma^0} = \frac{2B_0 m (4b_0 + 4b_D)}{F_\pi^2} \times 2M_\Sigma, \tag{A1f}$$

$$T_{\pi^0 \Xi^0} = \frac{2B_0 m (4b_0 + 2b_D - 2b_F)}{F_\pi^2} \times 2M_\Xi, \tag{A1g}$$

$$T_{\pi^0 \Xi^-} = \frac{2B_0 m (4b_0 + 2b_D - 2b_F)}{F_\pi^2} \times 2M_\Xi. \tag{A1h}$$

For $\langle \bar{u}u + \bar{s}s \rangle$, we use the T-matrices of the kaon–baryon:

$$T_{K^+p} = \frac{B_0(m + m_s)(4b_0 + 4b_D)}{F_K^2} \times 2M_N, \tag{A2a}$$

$$T_{K^+n} = \frac{B_0(m + m_s)(4b_0 + 2b_D - 2b_F)}{F_K^2} \times 2M_N, \tag{A2b}$$

$$T_{K^+\Lambda} = \frac{B_0(m + m_s)\left(4b_0 + \frac{10}{3}b_D\right)}{F_K^2} \times 2M_\Lambda, \tag{A2c}$$

$$T_{K^+\Sigma^+} = \frac{B_0(m + m_s)(4b_0 + 2b_D + 2b_F)}{F_K^2} \times 2M_\Sigma, \tag{A2d}$$

$$T_{K^+\Sigma^-} = \frac{B_0(m + m_s)(4b_0 + 2b_D - 2b_F)}{F_K^2} \times 2M_\Sigma, \tag{A2e}$$

$$T_{K^+\Sigma^0} = \frac{B_0(m + m_s)(4b_0 + 2b_D)}{F_K^2} \times 2M_\Sigma, \tag{A2f}$$

$$T_{K^+\Xi^0} = \frac{B_0(m + m_s)(4b_0 + 2b_D + 2b_F)}{F_K^2} \times 2M_\Xi, \tag{A2g}$$

$$T_{K^+\Xi^-} = \frac{B_0(m + m_s)(4b_0 + 4b_D)}{F_K^2} \times 2M_\Xi. \tag{A2h}$$

References

[1] K. Suzuki, M. Fujita, H. Geissel, H. Gilg, A. Gillitzer, R.S. Hayano, S. Hirenzaki, K. Itahashi, M. Iwasaki, P. Kienle, et al., Phys. Rev. Lett. **92**, 072302 (2004), [arXiv:nucl-ex/0211023].

[2] E. Friedman, M. Bauer, J. Breitschopf, H. Clement, H. Denz, E. Doroshkevich, A. Erhardt, G.J. Hofman, R. Meier, G.J. Wagner, et al., Phys. Rev. Lett. **93**, 122302 (2004), [arXiv:nucl-ex/0404031].

[3] E. E. Kolomeitsev, N. Kaiser, and W. Weise, Phys. Rev. Lett. **90**, 092501 (2003), [arXiv:nucl-th/0207090].

[4] D. Jido, T. Hatsuda, and T. Kunihiro, Phys. Lett. B **670**, 109 (2008), [arXiv:0805.4453] [Search in SPIRE].

[5] E. G. Drukarev and E. M. Levin, Nucl. Phys. A **511**, 679 (1990); **516**, 715 (1990) [erratum].

[6] E. G. Drukarev and E. M. Levin, Prog. Part. Nucl. Phys. **27**, 77 (1991).

[7] J. Gasser, H. Leutwyler, and M. E. Sainio, Phys. Lett. B **253**, 252 (1991).

[8] J. M. Alarcon, J. Martin Camalich, and J. A. Oller, Phys. Rev. D **85**, 051503 (2012), [arXiv:1110.3797] [Search inSPIRE].

[9] Y.-H. Chen, D.-L. Yao, and H. Q. Zheng, Phys. Rev. D **87**, 054019 (2013), [arXiv:1212.1893] [Search inSPIRE].

[10] M. Hoferichter, J. Ruiz de Elvira, B. Kubis, and U.-G. Meißner, Phys. Rev. Lett. **115**, 092301 (2015), [arXiv:1506.04142] [Search inSPIRE].

[11] D.-L. Yao, D. Siemens, V. Bernard, E. Epelbaum, A. M. Gasparyan, J. Gegelia, H. Krebs, and U.-G. Meißner, J. High Energy Phys. **1605**, 038 (2016), [arXiv:1603.03638] [Search inSPIRE].

[12] J. R. de Elvira, M. Hoferichter, B. Kubis, and U.-G. Meißner, J. Phys. G **45**, 024001 (2018), [arXiv:1706.01465] [Search inSPIRE].

[13] N. Kaiser, P. de Homont, and W. Weise, Phys. Rev. C **77**, 025204 (2008), [arXiv:0711.3154] [Search inSPIRE].

[14] S. Goda and D. Jido, Phys. Rev. C **88**, 065204 (2013), [arXiv:1308.2660] [Search inSPIRE].

[15] S. Hübsch and D. Jido, Phys. Rev. C **104**, 015202 (2021), [arXiv:2103.08823].

[16] J. A. Oller, Phys. Rev. C **65**, 025204 (2002), [arXiv:hep-ph/0101204].

[17] U. G. Meissner, J. A. Oller, and A. Wirzba, Ann. Phys. **297**, 27 (2002), [arXiv:nucl-th/0109026].

[18] N. Kaiser and W. Weise, Phys. Lett. B **671**, 25 (2009), [arXiv:0808.0856].

[19] B. R. Martin, Nucl. Phys. B **94**, 413 (1975).

[20] A. D. Martin, Nucl. Phys. B **179**, 33 (1981).

[21] K. Nakajima, N. Kim, S. Kobayashi, A. Masaike, A. Murakami, A. de Lesquen, K. Ogawa, M. Sakuda, F. Takasaki, and Y. Watase, Phys. Lett. B **112**, 80 (1982).

[22] J. S. Hyslop, R. A. Arndt, L. D. Roper, and R. L. Workman, Phys. Rev. D **46**, 961 (1992).

[23] W. R. Gibbs and R. Arceo, Phys. Rev. C **75**, 035204 (2007), [arXiv:nucl-th/0611095].

[24] K. Aoki and D. Jido, PTEP **2017**, 103D01 (2017); **2019**, 069201 (2019) [erratum], [arXiv:1705.07548] [Search inSPIRE].

[25] K. Aoki and D. Jido, PTEP **2019**, 013D01 (2019), [arXiv:1806.00925] [Search inSPIRE].

[26] T. Hyodo, S.-i. Nam, D. Jido, and A. Hosaka, Prog. Theor. Phys. **112**, 73 (2004), [arXiv:nucl-th/0305011].

[27] S. Weinberg, Phys. Rev. Lett. **17**, 616 (1966).

[28] T. Hyodo and D. Jido, Prog. Part. Nucl. Phys. **67**, 55 (2012), [arXiv:1104.4474] [Search inSPIRE].

[29] J. A. Oller, M. Verbeni, and J. Prades, J. High Energy Phys. **0609**, 079 (2006), [arXiv:hep-ph/0608204].

[30] L. Geng, Front. Phys. (Beijing) **8**, 328 (2013), [arXiv:1301.6815] [Search inSPIRE].

[31] K. Hashimoto, Phys. Rev. C **29**, 1377 (1984).

[32] A. S. Carroll, T. F. Kycia, K. K. Li, D. N. Michael, P. M. Mockett, D. C. Rahm, and R. Rubinstein, Phys. Lett. B **45**, 531 (1973).

[33] M. A. Luty and M. J. White, Phys. Lett. B **319**, 261 (1993), [arXiv:hep-ph/9305203].

[34] W. Cameron, A.A. Hirata, R. Jennings, W.T. Morton, E. Cazzoli, G. Giacomelli, P. Lugaresi-Serra, G. Mandrioli, A. Minguzzi-Ranzi, E. Castelli, et al., Nucl. Phys. B **78**, 93 (1974).

[35] BGRT Collaboration, G. Giacomelli, P. Lugaresi-Serra, G. Mandrioli, A. Minguzzi-Ranzi, A.M. Rossi, F. Griffiths, A.A. Hirata, R. Jennings, B.C. Wilson, et al., Nucl. Phys. B **56**, 346 (1973).

[36] C. J. S. Damerell, M.J. Hotchkiss, F. Wickens, K.R. Bentley, J.D. Davies, J.D. Dowell, R.J. Homer, C. McLeod, T.J. McMahon, H.B. Van der Raay, et al., Nucl. Phys. B **94**, 374 (1975).

[37] D. V. Bugg, R.S. Gilmore, K.M. Knight, D.C. Salter, G.H. Stafford, E.J.N. Wilson, J.D. Davies, J.D. Dowell, P.M. Hattersley, R.J. Homer, et al., Phys. Rev. **168**, 1466 (1968).

[38] T. Bowen, P. K. Caldwell, F. N. Dikmen, E. W. Jenkins, R. M. Kalbach, D. V. Petersen, and A. E. Pifer, Phys. Rev. D **2**, 2599 (1970).

[39] C. J. Adams, J.D. Davies, J.D. Dowell, G.H. Grayer, P.M. Hattersley, R.J. Howells, C. McLeod, T.J. McMahon, H.B. van der Raay, L. Rob, et al., Phys. Rev. D **4**, 2637 (1971).

[40] T. Bowen, E. W. Jenkins, R. M. Kalbach, D. V. Petersen, A. E. Pifer, and P. K. Caldwell, Phys. Rev. D **7**, 22 (1973).

[41] G. Ecker, J. Gasser, A. Pich, and E. de Rafael, Nucl. Phys. B **321**, 311 (1989).

[42] B. Kubis and U. G. Meissner, Eur. Phys. J. C **18**, 747 (2001), [arXiv:hep-ph/0010283].

[43] M. Holmberg and S. Leupold, Eur. Phys. J. A **54**, 103 (2018), [arXiv:1802.05168] [Search inSPIRE].

[44] E. Friedman and A. Gal, Phys. Lett. B **792**, 340 (2019), [arXiv:1901.03130] [Search inSPIRE].

[45] J.-X. Lu, L.-S. Geng, X.-L. Ren, and M.-L. Du, Phys. Rev. D **99**, 054024 (2019), [arXiv:1812.03799] [Search inSPIRE].

[46] J. K. Ahn and S. H. Kim, J. Korean Phys. Soc. **82**, 579 (2023).

[47] M. Amaryan et al., arXiv:2008.08215[Search inSPIRE].

[48] D. Jido, T. Hatsuda, and T. Kunihiro, Phys. Rev. D **63**, 011901 (2001), [arXiv:hep-ph/0008076].

[49] D. Jido, T. Hatsuda, and T. Kunihiro, Prog. Theor. Phys. Suppl. **168**, 478 (2007), [arXiv:0706.0258] [Search inSPIRE].

[50] S. Goda and D. Jido, PTEP **2014**, 033D03 (2014), [arXiv:1312.0832] [Search inSPIRE].

[51] D. Jido, JPS Conf. Proc. **17**, 081002 (2017), [arXiv:1603.07083] [Search inSPIRE].

[52] P. B. Siegel, W. B. Kaufmann, and W. R. Gibbs, Phys. Rev. C **31**, 2184 (1985).

[53] W. Weise, Nuovo Cimento A **102**, 265 (1989).

[54] R. Weiss, J. Aclander, J. Alster, M. Barakat, S. Bart, R.E. Chrien, R.A. Krauss, K. Johnston, I. Mardor, Y. Mardor, et al., Phys. Rev. C **49**, 2569 (1994).

[55] E. Friedman, A. Gal, and J. Mares, Nucl. Phys. A **625**, 272 (1997), [arXiv:nucl-th/9705026].